Cell Research

www.nature.com/cr
www.cell-research.com

ARTICLE

Lysine 2-hydroxyisobutyrylation of NAT10 promotes cancer metastasis in an ac4C-dependent manner

Long Liao[1,2,8], Yan He[1,2,8], Shu-Jun Li[1,2,8], Xiao-Mei Yu[1,2,8], Zhi-Chao Liu[3,8], Yi-Yao Liang[4], Han Yang[5], Jing Yang[1,2], Guo-Geng Zhang[1,2], Chun-Miao Deng[1], Xian Wei[1], Yi-Dong Zhu[1,2], Tao-Yang Xu[1,2], Can-Can Zheng[1], Chao Cheng[6], Ang Li[4], Zhi-Gang Li[3], Jin-Bao Liu[7] and Bin Li[1]✉

© The Author(s) under exclusive licence to Center for Excellence in Molecular Cell Science, Chinese Academy of Sciences 2023

Posttranslational modifications add tremendous complexity to proteomes; however, gaps remain in knowledge regarding the function and regulatory mechanism of newly discovered lysine acylation modifications. Here, we compared a panel of non-histone lysine acylation patterns in metastasis models and clinical samples, and focused on 2-hydroxyisobutyrylation (Khib) due to its significant upregulation in cancer metastases. By the integration of systemic Khib proteome profiling in 20 paired primary esophageal tumor and metastatic tumor tissues with CRISPR/Cas9 functional screening, we identified N-acetyltransferase 10 (NAT10) as a substrate for Khib modification. We further showed that Khib modification at lysine 823 in NAT10 functionally contribute to metastasis. Mechanistically, NAT10 Khib modification enhances its interaction with deubiquitinase USP39, resulting in increased NAT10 protein stability. NAT10 in turn promotes metastasis by increasing NOTCH3 mRNA stability in an N4-acetylcytidine-dependent manner. Furthermore, we discovered a lead compound #7586-3507 that inhibited NAT10 Khib modification and showed efficacy in tumor models in vivo at a low concentration. Together, our findings bridge newly identified lysine acylation modifications with RNA modifications, thus providing novel insights into epigenetic regulation in human cancer. We propose that pharmacological inhibition of NAT10 K823 Khib modification constitutes a potential anti-metastasis strategy.

Cell Research (2023) 33:355–371; https://doi.org/10.1038/s41422-023-00793-4

INTRODUCTION

Posttranslational modifications (PTMs) significantly increase complexity from the genome level to the proteome level.[1] During the past two decades, tremendous advances have been made in revealing the scope of non-histone protein acetylation.[2,3] A large number of novel lysine acylation modifications have recently been identified, but little is known about their biological functions in cancer.

Metastasis is a major cause of cancer deaths and consists of multiple cellular biological events termed the invasion-metastasis cascade. Although some mutations in certain genes have been identified in cancers,[4–6] including esophageal squamous cell carcinoma (ESCC),[7] genomic alterations cannot completely account for the mechanisms underlying cancer progression. Therefore, it is of the utmost urgency to identify novel therapeutic targets and effective biomarkers to improve the treatment outcomes of metastatic cancers.[8]

In a manner analogous to DNA and proteins, RNA can be modified posttranscriptionally through chemical modification of ribonucleosides, expanding the regulatory content embedded in RNA structure and function. N4-acetylcytidine (ac4C) modification is an ancient and conserved RNA modification, and early studies reported that ac4C was present mainly in tRNA and 18S rRNA.[9–11] Recently, ac4C was identified as the sole acetylation event in eukaryotic RNA and is present in mRNAs at physiologically relevant levels.[12] However, the biological function and mRNA substrates of ac4C modification in cancer remain largely unknown. To date, N-acetyltransferase 10 (NAT10) is the only reported enzyme responsible for ac4C deposition. However, the underlying mechanism by which aberrant ac4C modifications facilitate the invasion and metastasis of cancer remains to be elucidated.

In the present study, among the newly identified lysine acylation modifications examined, only the level of lysine 2-hydroxyisobutyrylation (Khib) was significantly different in highly metastatic ESCC cell sublines and metastatic tumor tissues. By integrating the systemic Khib proteome profiling in 20 paired primary ESCC tumor and metastatic tumor tissues with a CRISPR/Cas9 functional screening, we identify the RNA acetyltransferase

[1]Key Laboratory of Biological Targeting Diagnosis, Therapy and Rehabilitation of Guangdong Higher Education Institutes, State Key Laboratory of Respiratory Disease, The Fifth Affiliated Hospital of Guangzhou Medical University, Guangzhou, Guangdong, China. [2]MOE Key Laboratory of Tumor Molecular Biology, National Engineering Research Center of Genetic Medicine, College of Life Science and Technology, Jinan University, Guangzhou, Guangdong, China. [3]Department of Thoracic Surgery, Shanghai Chest Hospital, School of Medicine, Shanghai Jiao Tong University, Shanghai, China. [4]Key Laboratory of CNS Regeneration, Ministry of Education, Guangdong Key Laboratory of Non-Human Primate Research, Guangdong-Hong Kong-Macau Institute of CNS Regeneration, Jinan University, Guangzhou, Guangdong, China. [5]Department of Thoracic Surgery, Sun Yat-sen University Cancer Center, Guangzhou, Guangdong, China. [6]Department of Thoracic Surgery, The First Affiliated Hospital of Sun Yat-sen University, Guangzhou, Guangdong, China. [7]Guangdong Provincial Key Laboratory of Protein Modification and Degradation, State Key Laboratory of Respiratory Disease, and School of Basic Medical Sciences, Guangzhou Medical University, Guangzhou, Guangdong, China. [8]These authors contributed equally: Long Liao, Yan He, Shu-Jun Li, Xiao-Mei Yu, Zhi-Chao Liu.
✉email: lib2128@163.com

Received: 28 September 2022 Accepted: 8 February 2023
Published online: 8 March 2023

enzyme NAT10 as a non-histone substrate for Khib modification. We reveal the biological and clinical significance of NAT10 K823 Khib modification in cancer and identify lysine acetyltransferase 7 (KAT7) and sirtuin 7 (SIRT7) as writer and eraser for Khib deposition and removal, respectively. We further show that Khib modification at K823 in NAT10 is a potential driver event in cancer metastasis. Mechanistically, NAT10 Khib modification enhances its interaction with deubiquitinase USP39, resulting in increased NAT10 protein stability. Consequently, NAT10 increases NOTCH3 mRNA stability in an ac4C-dependent manner promoting metastasis. Furthermore, pharmacological inhibition of NAT10 Khib modification with a lead compound suggests a potential therapeutic strategy against cancer metastasis.

RESULTS

Comprehensive landscape of Khib in paired ESCC lymph node metastases

To investigate the importance of PTMs in ESCC metastasis, a panel of pan antibodies against 9 newly discovered lysine acylation modifications,[13–16] as well as dimethyllysine and trimethyllysine, were used to determine the PTM pattern in in-house-established highly invasive and metastatic ESCC cell sublines in vitro and in vivo (Supplementary information, Fig. S1a). We observed an obvious increase only in Khib but not in other PTMs in the highly invasive and metastatic ESCC cell sublines compared with the corresponding parental cells (Supplementary information, Fig. S1b). We obtained consistent results in matched ESCC and metastatic tissues, as well as in colorectal cancer and lung cancer cells and tissues, suggesting the consistency and universality of this phenomenon (Supplementary information, Fig. S1c–g). To obtain the global landscape of Khib in ESCC metastasis, 20 cases of primary ESCC tumor tissue (T), matched normal tissue (N) and lymph node metastatic tissue (LN) were subjected to systematic proteomic and quantitative Khib proteomic analyses (Fig. 1a, b). Excellent reproducibility, as assessed by the relative standard deviation (RSD) and the Pearson correlation coefficient (PCC) (Supplementary information, Figs. S2a, b, S3a, b), was maintained across the proteomic and Khib proteomic datasets. Principal component analysis (PCA) of the proteomic and Khib proteomic data showed that the N samples were clustered together and clearly separated from the T samples and LN samples (Fig. 1c). Sample quality control (QC) was also performed and found to be appropriate across the proteomic and Khib proteomic datasets, including the peptide length distribution (Supplementary information, Figs. S2c, S3c), protein coverage (Supplementary information, Fig. S2d), molecular weight distribution (Supplementary information, Fig. S2e) and number of peptides (Supplementary information, Fig. S2f). Proteomic analysis quantified 6841 proteins (Fig. 1d). As shown in Supplementary information, Fig. S2g, h, differentially expressed proteins (DEPs) include: 1552 upregulated and 548 downregulated proteins in the T vs N samples, and 2026 upregulated and 760 downregulated proteins in the LN vs N samples. Further analysis revealed the cellular distribution of the DEPs (Supplementary information, Fig. S2i, j). Gene Ontology (GO) enrichment analyses were performed and showed the possible functions of the DEPs in the T vs N and LN vs N sample proteomes (Supplementary information, Fig. S2k, l). Khib proteomic analysis quantified 5384 proteins and 39,997 Khib sites (Fig. 1d). Among the Khib sites, 7627 upregulated differentially expressed Khib sites (DEKSs) in 2424 proteins and 527 downregulated DEKSs in 392 proteins were identified in the T vs N sample proteomes, 5798 upregulated DEKSs in 1881 proteins and 956 downregulated DEKSs in 638 proteins were identified in the LN vs N sample proteomes (Supplementary information, Fig. S3d, e). EuKaryotic Orthologous Groups (KOG) classification and Kyoto Encyclopedia of Genes and Genomes (KEGG) enrichment analysis also revealed that Khib may be functionally involved in various biological processes and pathways (Supplementary information, Fig. S3f–i). Importantly, we defined 3 major distinct proteomic subgroups (Cluster 1, Cluster 2 and Cluster 3) by cluster analysis based on the proteomic and Khib proteomic data (Supplementary information, Tables S1, S2), and the DEPs and differentially expressed Khib-modified proteins (DEKPs) in Cluster 3 were upregulated in both metastatic tumor and primary tumor tissues compared to the matched normal tissues. We determined the overlap between Cluster 3 in the proteome and the Khib proteome (Fig. 1e), and 211 proteins were identified. Further GO enrichment analysis of the overlapping proteins demonstrated that the DEKPs related to cancer progression were enriched mainly in nucleic acid and RNA processing pathways (Fig. 1f). The sets of proteins in the nucleic acid and RNA processing pathways were extracted, and a protein–protein interaction (PPI) network was generated with the STRING database (Fig. 1g). Notably, the heatmap showed the top 20 altered proteins in the representative pathways according to the maximal clique centrality (MCC) algorithm (Fig. 1h), suggesting their important role in cancer metastasis.

Integration of proteomic analysis with CRISPR/Cas9 functional screening suggests that Khib modification of NAT10 at K823 may play a role in cancer metastasis

We further mapped the Khib proteome in KYSE150-Luc-LM5 cells, and the number of Khib sites per protein and peptide length distribution were shown in Supplementary information, Fig. S4a, b. A total of 139 DEKPs and 173 DEKSs were identified by proteomic analysis (Fig. 2a and Supplementary information, Table S3). Further bioinformatic analysis revealed the cellular distribution of the DEKPs (Fig. 2b). In addition, Clusters of Orthologous Groups (COG)/KOG enrichment analyses suggested possible functions of Khib in multiple cellular processes (Fig. 2c). Meanwhile, we identified 139 DEKPs in KYSE150-Luc-LM5 cells compared with the KYSE150-Luc cells, among which 108 DEKPs (~77.7%) were also observed in LN tissues compared to primary tumor tissues, suggesting the consistence and importance of these DEKPs in tumor metastasis (Supplementary information, Table S4). To systematically identify the drivers of cancer metastasis, we generated a single-guide RNA (sgRNA) library targeting the 139 DEKPs and performed a CRISPR/Cas9 functional screening. A library containing 6 sgRNAs per gene in addition to nontargeting sgRNAs was transduced into KYSE150-Luc cells. After in vitro and in vivo selection, gDNA from invaded cells and metastatic cells in animal models was extracted for PCR amplification of the sgRNA-coding region followed by high-throughput sequencing analysis (Fig. 2d and Supplementary information, Fig. S4c) (details in Materials and methods). Further GO biological process enrichment analysis of the candidate genes showed that the RNA binding pathway was the top-ranked pathway (Fig. 2e and Supplementary information, Fig. S4d), highly consistent with the enrichment of DEKPs in nucleic acid and RNA processing pathways identified by analysis of clinical samples (Fig. 1g). After overlapping the 20 proteins included in Fig. 1h with the 38 proteins clustered in the RNA binding pathway shown in Fig. 2e, we focused our research on NAT10, the only reported key enzyme for RNA ac4C modification[17] (Fig. 2f).

Next, we explored the Khib sites in NAT10 with a function in cancer metastasis. Among the 12 Khib sites in NAT10 identified by Khib proteomic analysis (Fig. 2g), only lysine 823 in NAT10 (NAT10 K823) satisfied all the following criteria and was thus taken as our research focus, since its Khib modification 1) was gradually increased from N to T and from T to LN, 2) was increased in metastatic cells compared with the corresponding parental cells (Supplementary information, Table S3), and 3) was required for the function of NAT10 in promoting ESCC metastasis (Supplementary information, Fig. S4e, f). In addition, NAT10 K823 was highly evolutionarily conserved among different species (Fig. 2h). To further investigate the role of Khib modification at K823 in NAT10, a polyclonal antibody specifically recognizing Khib-modified NAT10 K823 (NAT10 K823-Khib) was generated. The ELISA and dot blot analysis showed that the signal of modified peptides was ten times

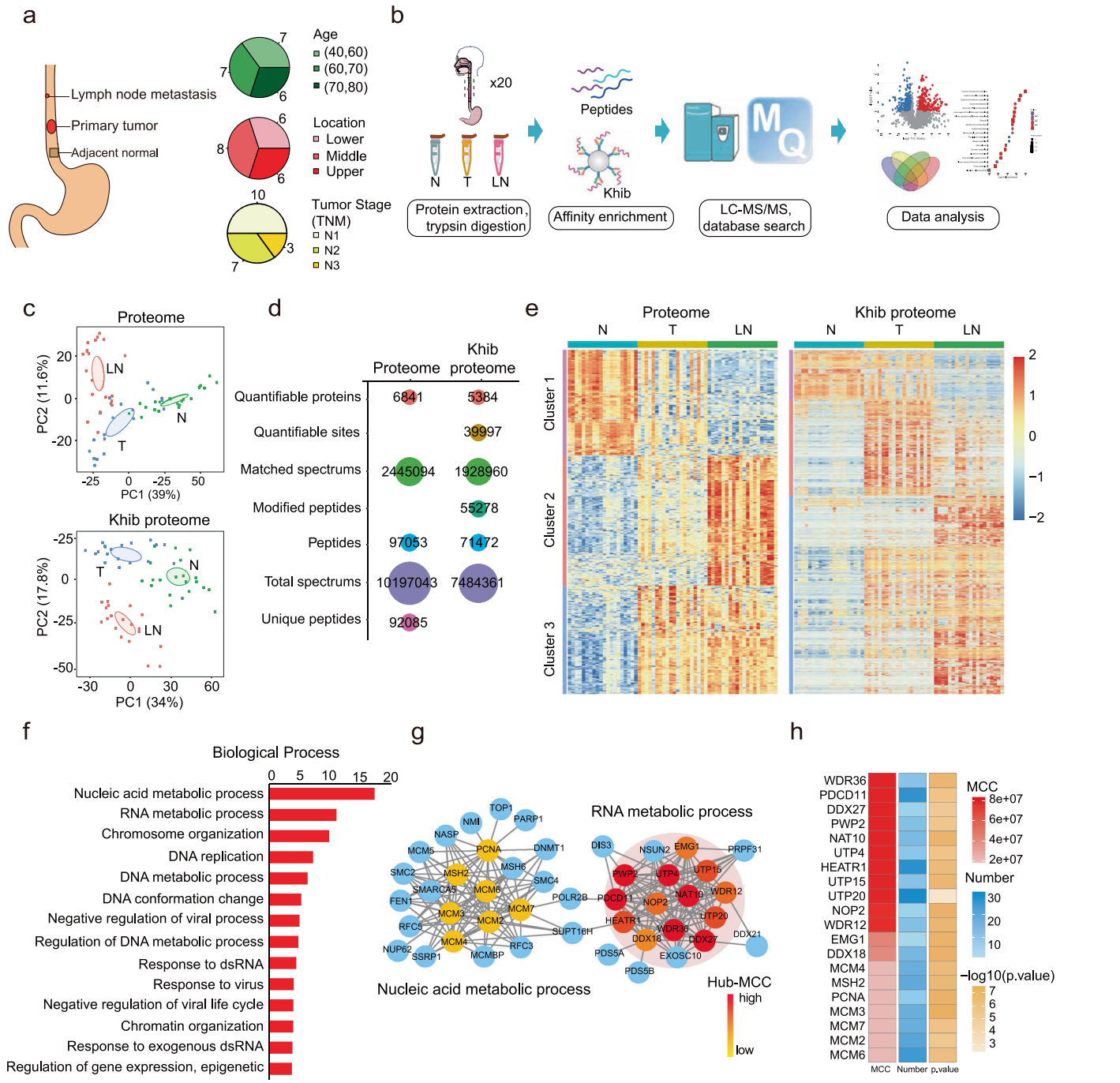

Fig. 1 Comprehensive landscape of Khib in ESCC metastatic cell lines and tissue samples. a Pie charts showing the age, tumor location and tumor stage of the 20 ESCC patients. **b** Schematic overview of the experimental design showing proteomic/Khib proteomic profiling based on 20 paired N/T/LN samples. **c** PCA plots showing the lack of a batch effect across all comparisons in the different data types; samples from each batch are represented by different colors. A clear separation is observed between the N, T, and LN samples in each data type. **d** Bubble chart showing the number of Khib-modified peptides, Khib sites and proteins identified by 4D MS. **e** DEPs and DEKPs identified by proteomic and Khib proteomic analyses of N, T and LN tissues were classified into three clusters. **f** Pathway analysis of overlapping proteins in cluster 3 identified by the proteomic and Khib proteomic analyses revealed RNA processing as the top protein-driven pathway. **g** PPI network showing the proteins clustered in the nucleic acid and RNA processing pathways and screening of hub genes using the MCC algorithm. **h** The top 20 proteins were significantly associated with the pathways indicated in **g**. The color gradient represents the MCC scores, numbers of mapped Khib sites, and significance levels.

stronger than that of non-modified peptides (Supplementary information, Fig. S4g, h). Further, the specific antibody against NAT10 K823-Khib can exclusively recognize the modified peptide PYDLK$_{hib}$RLEMYSRNC (K823$_{hib}$), not the unmodified peptide (PYDLKRLEMYSRNC) or the peptides with other modifications (Supplementary information, Fig. S4i). After visualizing blot on a fluorescent western blot imaging system, we found that NAT10 K823hib and NAT10 could be overlapped (Supplementary information, Fig. S4j). In addition, the antibody detected endogenous NAT10 K823hib in wild-type (WT) cells but not in NAT10-knockout

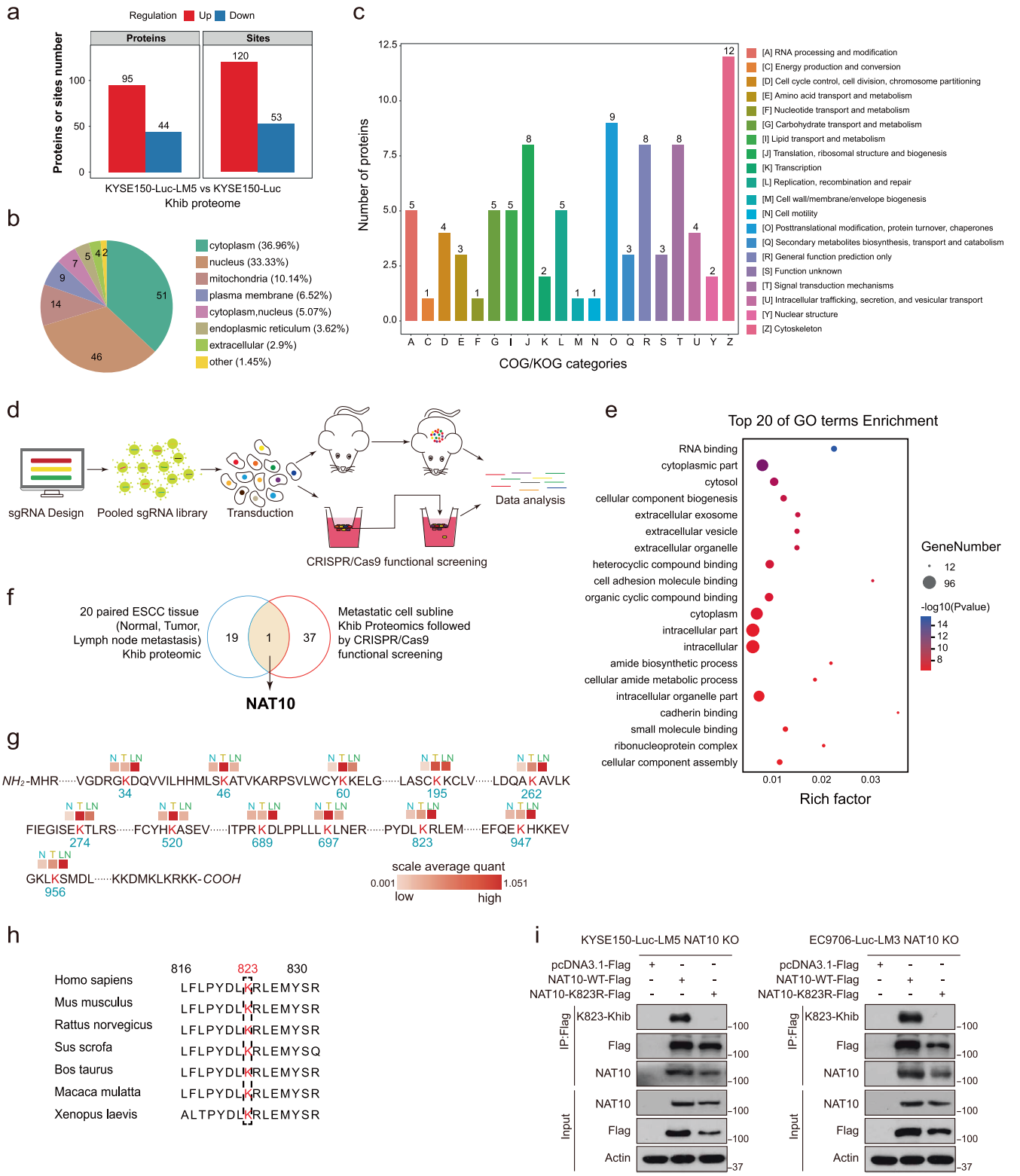

Fig. 2 Integration of proteomic analysis with CRISPR/Cas9 functional screening suggests that Khib modification of NAT10 at K823 is essential for cancer metastasis. a Statistical analysis of Khib-modified proteins and DEKSs in highly metastatic cell subline KYSE150-Luc-LM5. **b** Subcellular distribution of Khib-modified proteins. **c** COG/KOG enrichment analysis of Khib-modified proteins. **d** Schematic diagram showing the process for CRISPR/Cas9 screening of key regulators of tumor metastasis. Upper: cells were injected intravenously into NCG mice and lung with metastasis were sampled 4 weeks upon injection. Lower: in vitro screen via three rounds of invasion selection. **e** GO biological process enrichment analysis showed significant enrichment of the candidate genes in the RNA binding pathway. **f** Venn diagram showing the overlap of the genes associated with RNA binding and the top 20 altered proteins identified by the MCC algorithm (Fig. 1h). **g** Khib levels at 12 sites of NAT10 in 20 paired N/T/LN samples. **h** Alignment of protein sequences surrounding K823 in NAT10 among different species. **i** ESCC cells were transiently transfected with the pcDNA3.1, NAT10-WT or NAT10-K823R plasmid and were then subjected to immunoprecipitation/immunoblotting with the indicated antibodies.

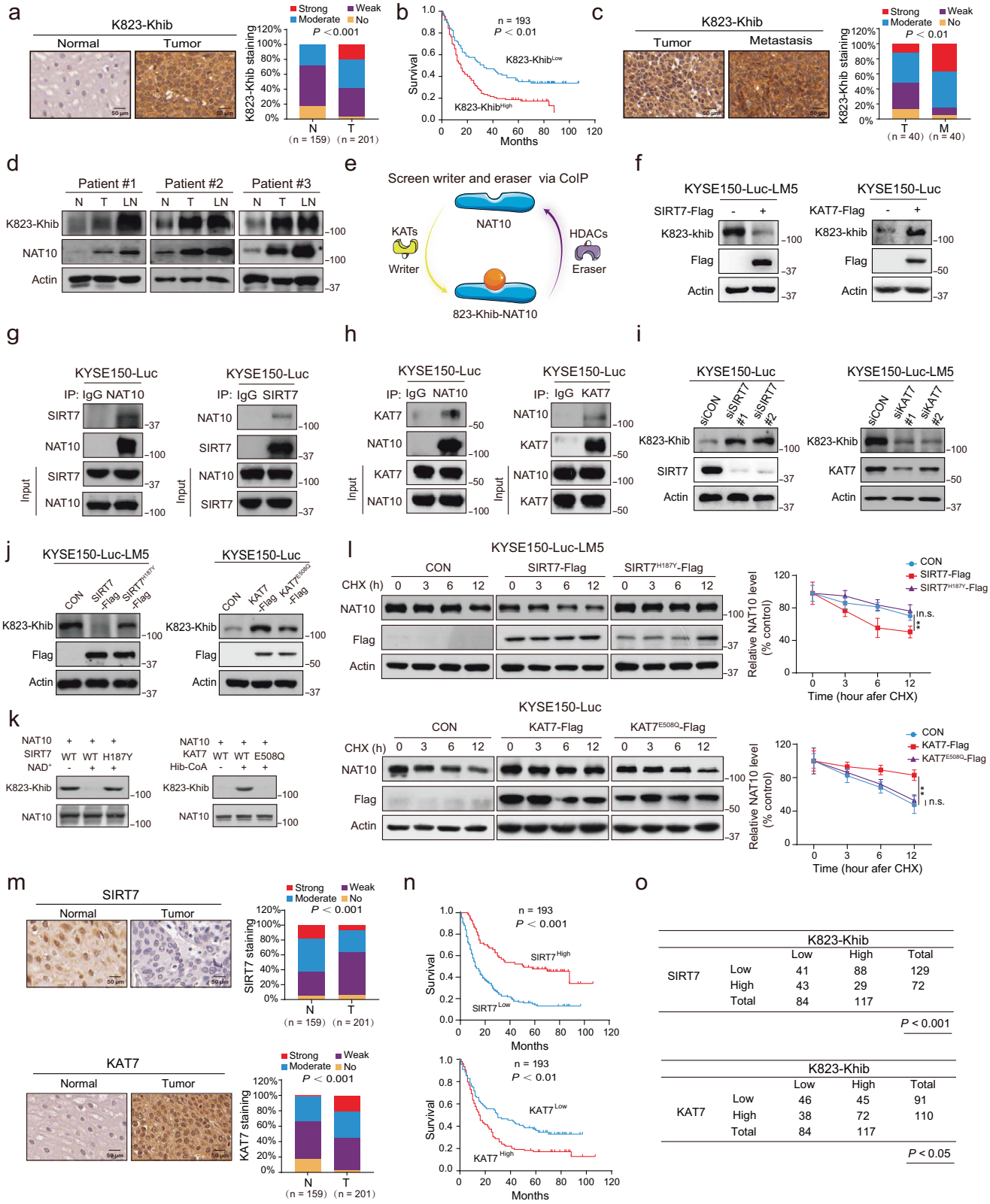

		K823-Khib		
		Low	High	Total
SIRT7	Low	41	88	129
	High	43	29	72
	Total	84	117	

$P < 0.001$

		K823-Khib		
		Low	High	Total
KAT7	Low	46	45	91
	High	38	72	110
	Total	84	117	

$P < 0.05$

(NAT10-KO) cells (Supplementary information, Fig. S4k). As shown in Fig. 2i, mutagenesis of K823 to R823 (lysine to arginine, mimicking the de-2-hydroxyisobutyrylation state) resulted in a greatly decreased K823-Khib level, supporting the hypothesis that K823 is the major functional Khib site in NAT10.

KAT7 and SIRT7 are the writer and eraser for Khib modification of NAT10

Given the striking potential significance of NAT10 Khib modification in cancer progression, we evaluated the clinical relevance of this modification. A tissue microarray containing 201 ESCC tissues and

Fig. 3 KAT7 and SIRT7 are the writer and eraser for Khib modification of NAT10, respectively. a Representative images and expression pattern of NAT10 K823-Khib in 201 ESCC and 159 paired adjacent normal tissues. **b** Kaplan–Meier analysis of overall survival for 193 ESCC patients stratified by the tumor NAT10 K823-Khib level. **c** Representative images and expression pattern of NAT10 K823-Khib in 40 primary ESCC and matched metastatic tumor tissues. **d** Expression of NAT10 K823-Khib and NAT10 in primary tumor tissues, matched adjacent normal tissues and metastatic LNs from ESCC patients. **e** Strategy used to identify the writer and eraser for NAT10 Khib modification. **f** Western blot analysis showing the effect of KAT7 or SIRT7 on the NAT10 K823-Khib level. **g** An immunoprecipitation assay was performed to confirm the endogenous interaction between NAT10 and SIRT7. **h** The interaction between endogenous NAT10 and KAT7 was investigated by immunoprecipitation. **i** Effect of SIRT7 knockdown or KAT7 knockdown on NAT10 K823-Khib levels. **j, k** Effect of the KAT7-E508Q and SIRT7-H187Y mutants on the NAT10 K823-Khib level in vivo and in vitro. **l** Analysis of protein stability after CHX treatment in ESCC cells transfected with WT SIRT7 or catalytically inactive SIRT7 (H187Y mutant) (upper panel). Analysis of protein stability after CHX treatment in ESCC cells transfected with WT KAT7 or HAT-dead KAT7 (E508Q mutant) (lower panel). **m** Representative images and expression pattern of SIRT7 and KAT7 in ESCC tissue arrays. **n** Kaplan–Meier analysis of overall survival for ESCC patients stratified by SIRT7 or KAT7 expression. **o** Association between the K823-Khib level and KAT7 or SIRT7 expression. Error bars, SDs; n.s. not significant; $^{**}P < 0.01$.

Table 1. Correlation between NAT10 K823-Khib levels and clinicopathological parameters in 201 patients with esophageal cancer.

Variable	*n*	Low K823-Khib	High K823-Khib	*P* value
Age (years)				
≤ 55	28	15	13	
> 55	173	69	104	0.173
Sex				
Female	42	23	19	
Male	159	61	98	0.055
T stage				
1/2	42	22	20	
3/4	159	62	97	0.117
N stage				
N0	94	48	46	
N1/N2/N3	107	36	71	0.012
Grade				
I & II	160	73	87	
III & IV	41	11	30	0.029

159 matched adjacent normal tissues was used for immunohistochemical staining of NAT10 K823-Khib. An increased NAT10 K823-Khib level was frequently observed in tumor tissues (58.2%, 117/201) compared with normal tissues (28.3%, 45/159) ($P < 0.001$, Fig. 3a), and a high NAT10 K823-Khib level was significantly associated with pathological N stage and tumor grade ($P < 0.05$, Table 1). Kaplan–Meier survival analysis indicated that patients with high NAT10 K823-Khib levels exhibited markedly shorter survival times (median survival time = 15.0 months) than patients with low NAT10 K823-Khib levels (median survival time = 33.0 months) (log-rank test, $P < 0.01$; Fig. 3b). Moreover, immunohistochemical analysis of NAT10 K823-Khib in another tissue microarray consisting of 40 pairs of primary ESCC tumor and matched metastatic tumor tissues showed that most of the metastatic tumor tissues had a higher NAT10 K823-Khib level than the matched primary tumor tissues (Fig. 3c). Western blot analysis of the clinical specimens was performed using an antibody specific for NAT10 K823-Khib, further confirming that Khib modification at K823 in NAT10 was upregulated in primary ESCC tumor and matched metastatic tumor tissues compared with adjacent normal tissues (Fig. 3d).

The balance between protein acetylation and deacetylation is maintained by two classes of enzymes, histone acetyltransferases (HATs) and histone deacetylases (HDACs).[18] To identify the deacylases responsible for removing NAT10 Khib modification, the association of a series of HDACs, including HDAC 1–11 and sirtuin (SIRT) 1–7, with NAT10 was tested by immunoprecipitation (IP) (Fig. 3e). SIRT1, SIRT7, and HDAC4 were found to interact with NAT10 (Supplementary information, Fig. S5a, b). Western blot analysis of NAT10 K823-Khib indicated that only SIRT7 but not the other HDACs deacylated NAT10 at K823 (Fig. 3f, left panel and Supplementary information, Fig. S5c). SIRT7 was confirmed to bind to NAT10 in ESCC cells by reciprocal co-immunoprecipitation (co-IP) (Fig. 3g and Supplementary information, Fig. S5d). On the other hand, screening of a panel of HATs showed that KAT7 interacted with NAT10 and enhanced its Khib modification (Fig. 3f, right panel and Supplementary information, Fig. S5e). The interaction between KAT7 and NAT10 was verified endogenously (Fig. 3h and Supplementary information, Fig. S5f). Interestingly, our results showed that KAT7 and SIRT7 had a slight effect on the global Khib level, whereas neither of their catalytically inactive mutants (KAT7-E508Q and SIRT7-H187Y) affected it (Supplementary information, Fig. S5g, h). Loss-of-function experiments further validated that NAT10 K823 can be deacylated by SIRT7 but acylated by KAT7 (Fig. 3i). More importantly, SIRT7 but not its H187Y[19] mutant decreased the NAT10 K823-Khib level in vivo and in vitro (Fig. 3j, k, left panel). Similarly, the E508Q[20] mutant of KAT7 lost the ability to regulate the NAT10 K823-Khib level in vivo and in vitro (Fig. 3j, k, right panel). Mechanistically, SIRT7 and KAT7 but not the corresponding acylation- or deacylation-deficient mutants, decreased and increased NAT10 protein stability, respectively (Fig. 3l). Furthermore, the expression patterns and clinical relevance of SIRT7 and KAT7 were assessed in the same ESCC tissue microarrays used above. SIRT7 expression was downregulated in ESCC tumor tissues and associated with favorable patient survival, whereas upregulation of KAT7 often predicted poor prognosis (Fig. 3m, n and Supplementary information, Tables S5, S6). More importantly, a negative correlation between the protein levels of SIRT7 and NAT10 K823-Khib was observed, and the KAT7 expression level was positively correlated with the NAT10 K823-Khib level (Fig. 3o). These data collectively indicate that Khib modification of NAT10 at K823 is controlled by KAT7 and SIRT7.

Identification of deubiquitinase USP39 as an interacting protein of NAT10

We next investigated whether Khib modification regulates NAT10 protein degradation and explored the mechanisms involved. A cycloheximide (CHX) chase assay was performed and showed that mutation of K823, the key Khib site in NAT10, significantly impaired NAT10 protein stability (Fig. 4a). To explore the mechanisms by which Khib modification regulates NAT10 protein stability, immunoprecipitation coupled with liquid chromatography-tandem mass spectrometry (IP-MS) was performed to identify the interacting partners of NAT10 (Fig. 4b, c). Among the 63 proteins identified (Supplementary information, Table S7), the only ubiquitin ligase or deubiquitinase was ubiquitin-specific protease 39 (USP39), which has been reported to function as a deubiquitinase to promote tumorigenesis.[21] To investigate the clinical significance of USP39 in ESCC, immunohistochemistry analysis was performed in the same tissue microarrays described above. We found that 55.2% (111/201) of tumor tissues showed high expression of USP39, whereas 23.2% (37/159) of non-tumor tissues showed high USP39 expression ($P < 0.001$) (Supplementary information, Fig. S6a). Kaplan–Meier

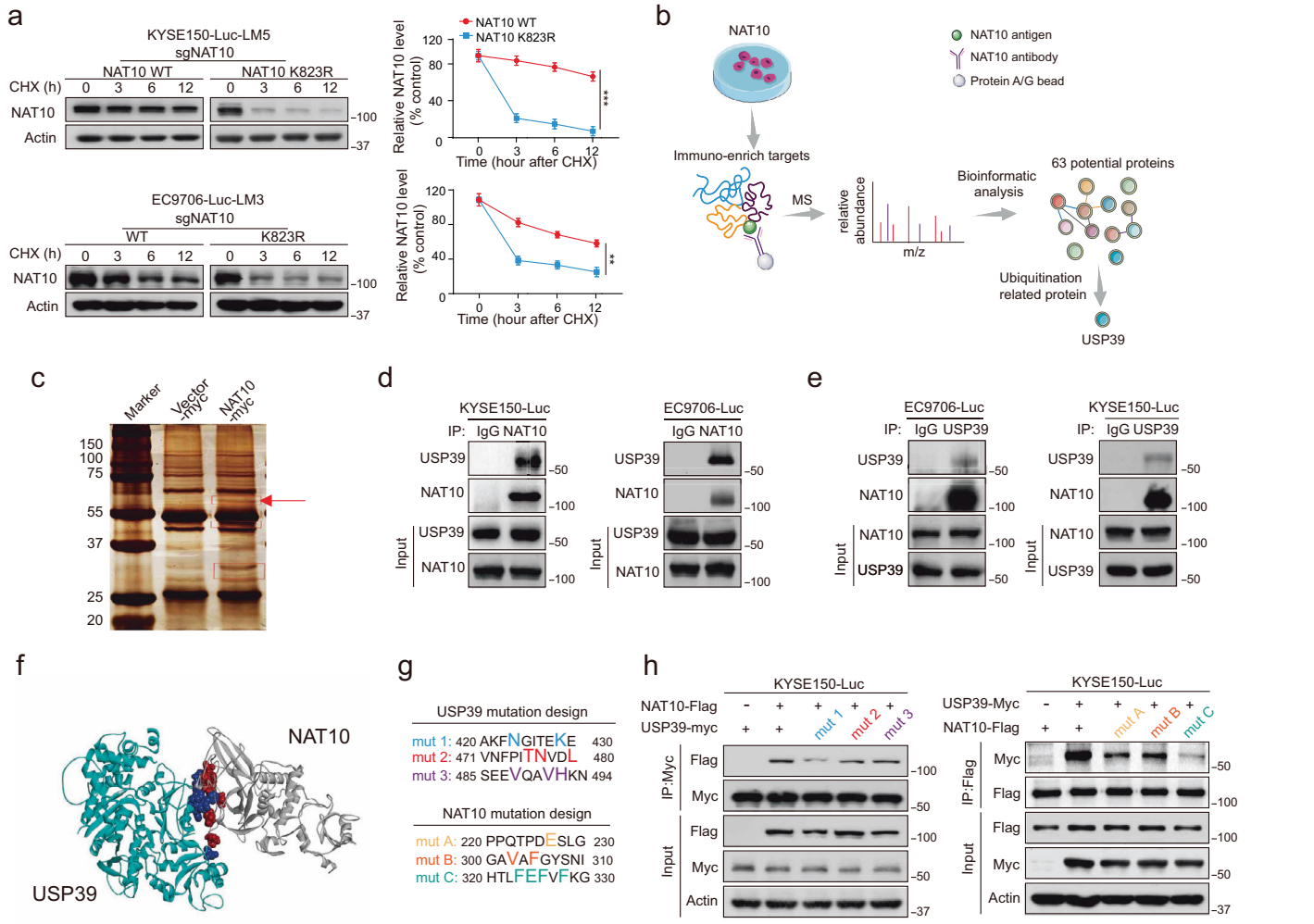

Fig. 4 Identification of deubiquitinase USP39 as an interacting protein of NAT10. a Analysis of protein stability after CHX treatment for the indicated times in NAT10-WT and NAT10-K823R cells. **b**, **c** IP-MS was performed to identify the interacting partners of NAT10. **d**, **e** Co-IP assay showing the endogenous interaction between NAT10 and USP39. **f** Molecular docking showing the interaction between NAT10 and USP39. **g** Diagram showing the design of the USP39 and NAT10 mutants. **h** Co-IP assay showing the binding between the NAT10 and USP39 mutants, as well as between the USP39 and NAT10 mutants. Error bars, SDs; $^{**}P < 0.01$; $^{***}P < 0.001$.

survival analysis demonstrated that patients with high tumor USP39 expression had shorter survival times (median survival time = 15.0 months) than patients with low tumor USP39 expression (median survival time = 28.5 months) (log-rank test, $P < 0.01$, Supplementary information, Fig. S6b and Table S8).

Our reciprocal co-IP experiments demonstrated the interaction between endogenous USP39 and NAT10 in ESCC cells (Fig. 4d, e), which was further confirmed with exogenously expressed USP39 and NAT10 (Supplementary information, Fig. S6c, d). To elucidate the binding sites involved in the interaction between USP39 and NAT10, molecular docking was performed, and we constructed 3 plasmids expressing different USP39 (mut #1, mut #2, mut #3) or NAT10 (mut #A, mut #B, mut #C) mutants to identify the amino acids constituting the key binding sites (Fig. 4f, g). The co-IP assays indicated that amino acids 423–428 (site #1) in USP39 and amino acids 323–327 (site #C) in NAT10 may be required for the binding of USP39 to NAT10 (Fig. 4h).

Stabilization of Khib-modified NAT10 by USP39 leads to its upregulation in ESCC

Western blot analysis showed that USP39 overexpression markedly increased NAT10 expression; in contrast, knockdown of USP39 greatly decreased NAT10 expression (Fig. 5a). Unlike WT USP39, the USP39-C306A mutant, which has been shown to lose deubiquitinase activity,[22] could not affect the expression level of NAT10 (Fig. 5b). Moreover, the results of the CHX chase and IP assays showed that ectopic expression of WT USP39 but not the USP39-C306A mutant decreased NAT10 ubiquitination level and increased NAT10 stability (Fig. 5c, d).

A systematic identification of USP39 substrates is lacking. Next, quantitative mass spectrometry (MS)-based ubiquitylome analysis was used to compare ubiquitinated proteins in USP39-overexpressing ESCC cells and control cells (Fig. 5e and Supplementary information, Fig. S7a, b). A total of 2138 DEPs were identified as potential substrates of USP39, and we identified 1002 sites with upregulated ubiquitination and 3822 sites with downregulated ubiquitination in USP39-overexpressing cells (Fig. 5f and Supplementary information, Table S9). As shown in Fig. 5g and Supplementary information, Fig. S7c, further bioinformatic analysis showed the top 10 reactome enrichment and cellular distribution of the DEPs in the ubiquitylome. To reveal biological processes associated with ubiquitinated proteins, we performed GO biological process term, and KEGG pathway and protein domain enrichment analyses followed by hierarchical

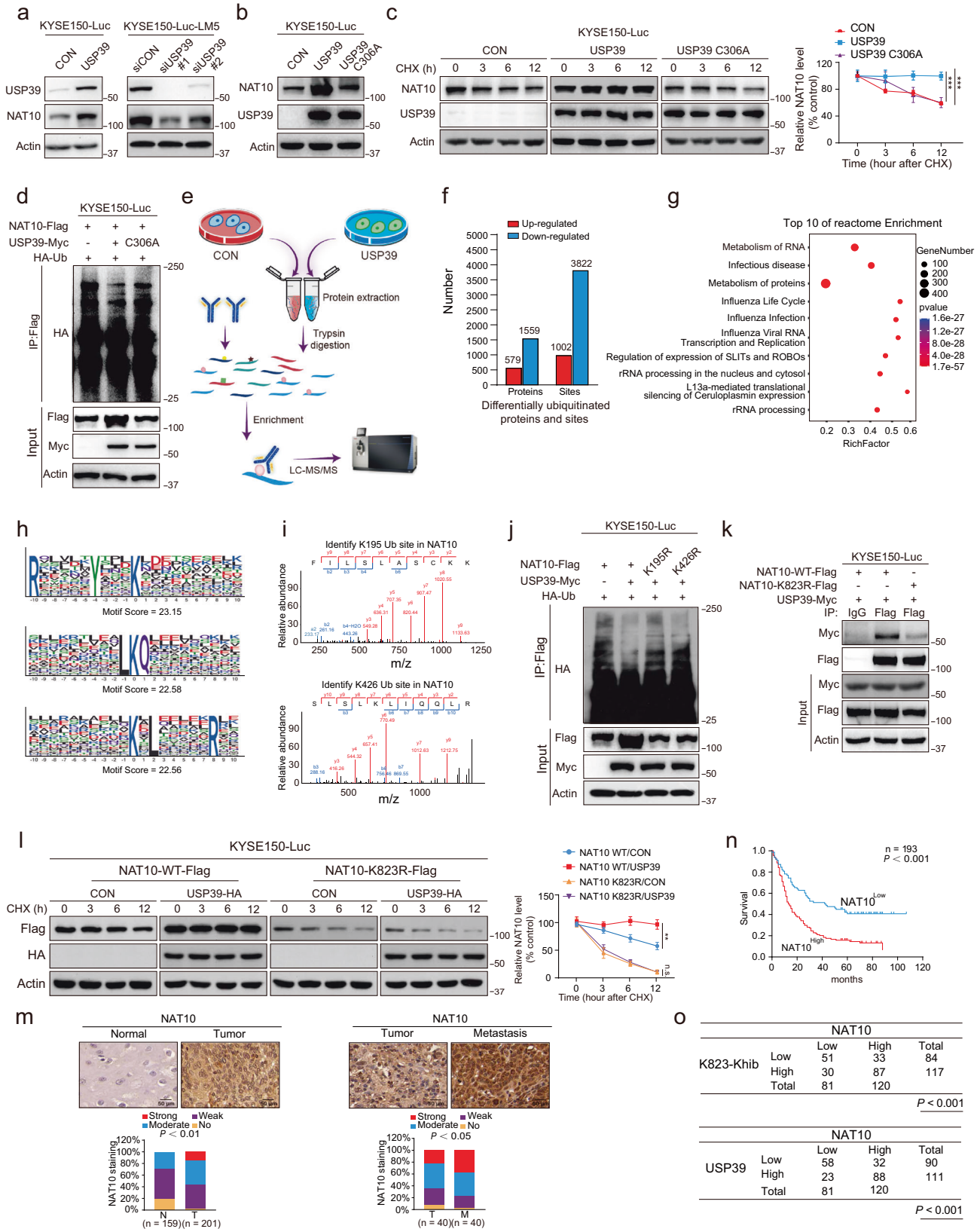

clustering (Supplementary information, Fig. S7d–h). Our analyses further supported the prevalent nature of USP39-mediated deubiquitination. The 3 most frequently observed motifs in the target proteins regulated by USP39 are shown in Fig. 5h. More importantly, the ubiquitylome data indicated that NAT10 is deubiquitinated at K195 and K426 by USP39 (Fig. 5i). As shown in Fig. 5j, USP39-induced deubiquitination of NAT10 was significantly attenuated when K195 or K426 was mutated,

Fig. 5 Stabilization of Khib-modified NAT10 by USP39 leads to its upregulation in ESCC. a Western blot analysis showing the effect of USP39 on NAT10 expression. **b** Expression of NAT10 after transfection with WT USP39 or the C306A mutant, which lacks deubiquitinase activity. **c** WT USP39 but not the C306A mutant decreased the degradation of NAT10 and increased its protein level. **d** Effect of USP39 and USP39-C306A on the ubiquitination of NAT10. **e** Experimental workflow for ubiquitinome enrichment via the UbiSite antibody and deep proteome analyses. **f** A set of the DEPs and ubiquitination site(s) were predicted by MS. **g** GO analysis of ubiquitinated proteins showing the top 10 enrichment functions. **h** Sequence logo of the ubiquitination site motif and conservation of ubiquitination sites identified by the motif-x program. **i** MS analysis showed that K195 was ubiquitinated at the peptide FILSLASCK(1)K and that K426 was ubiquitinated at the peptide SLSLK(1)LIQQLR. **j** USP39-mediated deubiquitination of NAT10 was significantly reduced in ESCC cells transfected with NAT10-K195R or NAT10-K426R. **k** ESCC cells co-transfected with USP39-Myc and NAT10-WT or the NAT10-K823R mutant were collected for immunoprecipitation analysis. **l** Analysis of protein stability after CHX treatment for the indicated times in NAT10-WT and NAT10-K823R cells. **m** Representative images and expression patterns of NAT10 in 201 ESCC and 159 paired normal tissues (left panel) as well as in 40 primary tumors and matched metastatic tumors (right panel). **n** Kaplan–Meier analysis of overall survival for 193 ESCC patients stratified by tumor NAT10 expression. **o** Association between NAT10 with K823-Khib or USP39 expression in ESCC tissues. Error bars, SDs; n.s. not significant; $^{**}P < 0.01$; $^{***}P < 0.001$.

supporting that K195 and K426 are the key ubiquitination sites in NAT10. These results strongly demonstrate the functional significance of USP39 in regulating the protein stability of NAT10.

Interestingly, mutation of NAT10 K823, the Khib modification site, dramatically inhibited its physical binding to USP39 (Fig. 5k). As shown in Fig. 5l, we further determined the protein stability in the cells overexpressing NAT10-WT or NAT10-K823R. Our results showed that overexpression of USP39 increased the stability of WT NAT10, but did not exert the similar effect on the mutant (NAT10-K823R). Similarly, ectopic expression of SIRT7, which decreased NAT10 K823-Khib level, significantly reduced the interaction between NAT10 and USP39 (Supplementary information, Fig. S7i), suggesting that the USP39–NAT10 interaction is dependent on Khib modification of NAT10.

Next, the expression level of NAT10 was assessed in the same tissue microarrays used above. Higher NAT10 expression was found in most of the tumor tissues than in the corresponding adjacent normal tissues ($P < 0.01$), and the metastatic tumor tissues had higher NAT10 levels than the primary tumor tissues (Fig. 5m). Consistent with these patterns, NAT10 expression was correlated with lymph node metastasis (Supplementary information, Table S10). Patients with low tumor NAT10 expression had better survival (median survival time = 42.5 months) than patients with high tumor NAT10 expression (median survival time = 13.5 months) (Fig. 5n). More importantly, the results showed that expression of NAT10 was not only positively correlated with the level of NAT10 K823-Khib, but also associated with USP39 expression in ESCC, further supporting our hypothesis that Khib modification at K823 contributes to the USP39-mediated stabilization of NAT10 protein (Fig. 5o).

Identification of NAT10 as a driver of cancer metastasis

To investigate the functional role of NAT10 in cancer metastasis, NAT10-overexpressing or NAT10-KO ESCC cell lines were generated, and their invasive and metastatic potential was compared with that of the corresponding control cells. The Boyden chamber invasion assay showed that ectopic expression of NAT10 markedly enhanced the invasion of ESCC cells (Fig. 6a). In addition, a footpad inoculation model was established, and swollen popliteal lymph nodes were observed in all (6/6) mice injected with NAT10-overexpressing ESCC cells but in only 33.3% (2/6) of the mice injected with control cells (Fig. 6b). Bioluminescence imaging data from the experimental metastasis model indicated that compared with intravenous injection of control cells, intravenous injection of NAT10-overexpressing ESCC cells resulted in increased lung metastasis in mice (Fig. 6c). Notably, overexpression of NAT10 induced epithelial-mesenchymal transition (EMT) in ESCC cells, as indicated by the upregulated fibronectin and downregulated E-cadherin expression, and the opposite results were observed in NAT10-KO cells (Fig. 6d). In addition, a significant increase in filopodia was observed in NAT10-overexpressing ESCC cells, while a reduction was detected in NAT10-KO cells (Supplementary information, Fig. S8a). These data suggested that NAT10 may promote cancer invasion and metastasis via fibronectin-mediated filopodia formation. The role of NAT10 in cancer was confirmed by loss-of-function experiments showing that knockout of NAT10 significantly suppressed ESCC cell invasion, lymph node metastasis and lung metastasis (Fig. 6e–g). Furthermore, WT NAT10 or the K823R mutant was re-overexpressed in NAT10-deficient ESCC cells, and the invasion and metastasis ability of these cells was then compared. WT NAT10 but not the K823R mutant abolished the suppressive effect of NAT10 knockout on ESCC cell invasion and metastasis. Overall, these results indicate that NAT10 is a vital regulator of cancer metastasis (Fig. 6h, i).

NAT10 catalyzes ac4C modification of NOTCH3 mRNA to increase its stability

NAT10 is the only identified acetyltransferase for mRNA ac4C modification, and we next integrated RNA sequencing (RNA-seq) and acetylated RNA immunoprecipitation and sequencing (acRIP-seq) to assess the existence of NAT10-regulated ac4C targets among mRNAs and lncRNAs (Fig. 7a). We performed RNA-seq in NAT10-overexpressing ESCC cells, and GO enrichment analysis revealed that numerous differentially expressed genes were involved in the regulation of transcription (Supplementary information, Fig. S9a, b). The average distribution of ac4C peaks was determined across mRNAs and lncRNAs in NAT10-overexpressing cells and control cells (Supplementary information, Fig. S9c). The ac4C sites were clustered proximal to translation start sites, with most peaks located within coding sequences (CDSs), based on acRIP-seq (Supplementary information, Fig. S9d). A total of 251 genes exhibited increased mRNA expression and ac4C modification levels in NAT10-overexpressing cells, and we focused on these genes (Fig. 7b and Supplementary information, Tables S11, S12). KEGG enrichment analysis indicated enrichment of the Notch signaling pathway in NAT10-overexpressing ESCC cells, prompting us to investigate whether NOTCH3 is a substrate of NAT10 and mediates its biological function in cancer metastasis (Fig. 7c). The quantitative real-time polymerase chain reaction (qRT-PCR) and western blot data showed that overexpression and knockout of NAT10 led to increased and decreased NOTCH3 expression, respectively, at both the mRNA and protein levels (Fig. 7d–f). The half-life of NOTCH3 mRNA was found to be longer in NAT10-overexpressing cells, and shorter in NAT10-deficient cells (Fig. 7g). The results of acRIP-qPCR indicated that more NOTCH3 mRNAs were pulled down with the anti-ac4C antibody in NAT10-overexpressing cells, and we obtained the opposite results in NAT10-KO cells (Fig. 7h). Unlike WT NAT10, the NAT10 G641E mutant with loss of acetyltransferase activity could not increase the ac4C enrichment or stability of NOTCH3 mRNA, suggesting that NAT10 increases NOTCH3 mRNA stability via ac4C modification[23] (Fig. 7i and Supplementary information, Fig. S9e–h). To verify the presence and exact location of the ac4C site in NOTCH3 mRNA, an orthogonal method with nucleotide resolution was performed. ac4C can be reduced to tetrahydro-ac4C using sodium borohydride ($NaBH_4$), resulting in C:T mismatches during first

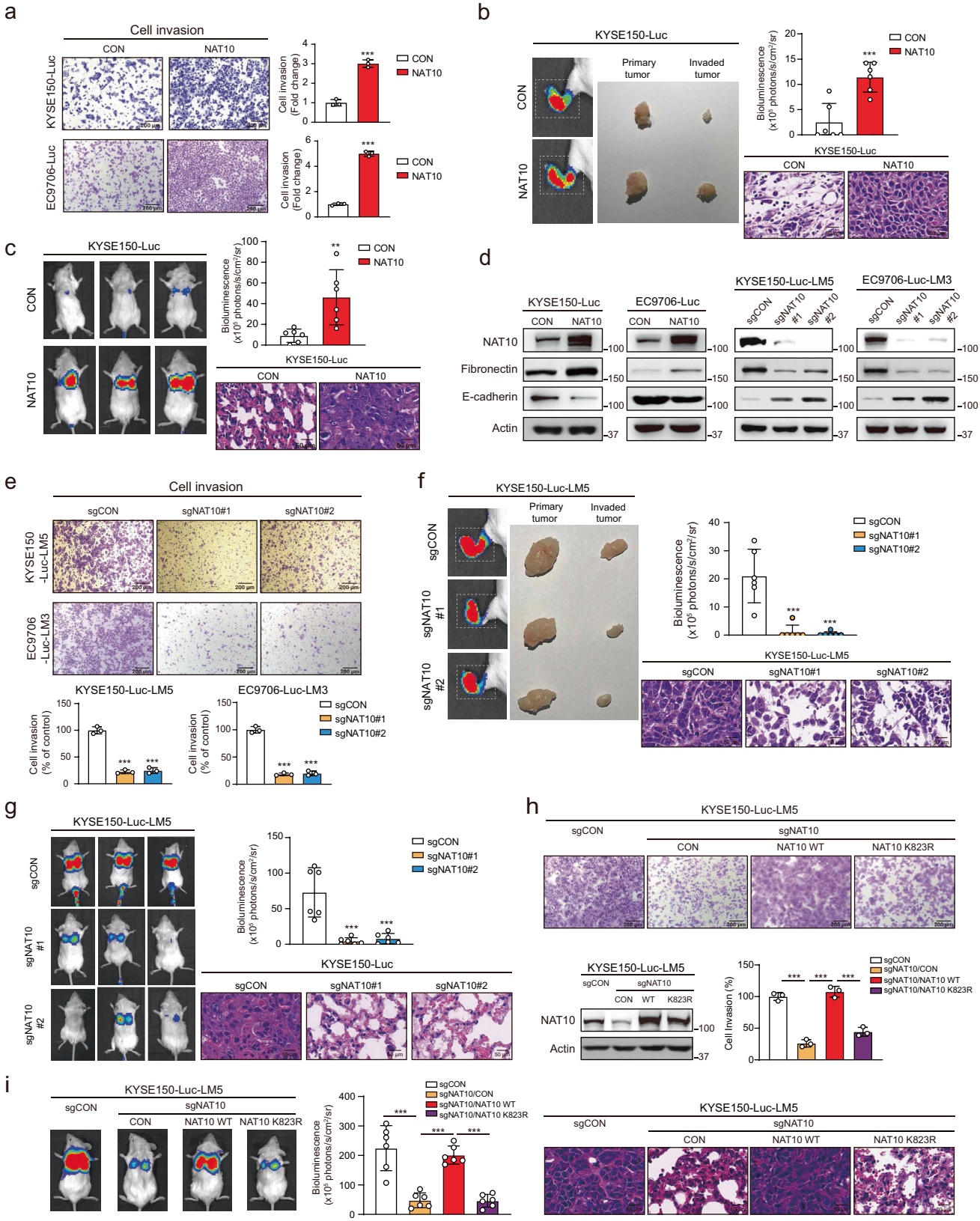

strand cDNA synthesis.[9,11,24] Sanger sequencing of cDNA showed an average of 28.4% C:T mismatchs in NOTCH3 mRNAs from $NaBH_4$-treated total RNAs in KYSE150-Luc-LM5 cells, supporting that NOTCH3 mRNA is indeed acetylated (Fig. 7j). Moreover, inhibition of NAT10 significantly decreased the C:T mismatches of acPeak region identified by acRIP-seq in NOTCH3 mRNA, and overexpression of WT NAT10 but not the NAT10 G641E mutant increased the C:T mismatches of acPeak region. In contrast, C:T

Fig. 6 NAT10 K823 is clinically and functionally important for ESCC metastasis. a Boyden chamber assay showing the effect of NAT10 overexpression on cell invasion. **b** Representative images and quantification of swollen inguinal LNs and primary tumors in mice following subcutaneous footpad injection of NAT10-overexpressing cells. **c** Bioluminescence imaging and quantification of lung metastasis in mice intravenously injected with NAT10-overexpressing cells. Hematoxylin-eosin (H&E) staining showing lung metastasis as indicated. **d** Western blot showing the effect of NAT10 overexpression or NAT10 knockout via a sgRNA targeting NAT10 on the EMT markers fibronectin and E-cadherin. **e**–**g** Cell invasion, lymph node metastasis and lung metastasis were monitored in ESCC cells with NAT10 knockout. **h** Boyden chamber assay showing that the NAT10 WT but not NAT10 K823R abolished the suppressive effect of NAT10 knockout on cell invasion. **i** Bioluminescence imaging and quantitative analysis showing that the NAT10 K823R mutation did not affect the inhibitory effect of NAT10 knockout on metastasis in mice. H&E staining showing lung metastasis as indicated. Error bars, SDs; $^{**}P < 0.01$; $^{***}P < 0.001$.

mismatch was not observed in the non-acPeak region of $NaBH_4$-treated total RNA (Fig. 7j and Supplementary information, Fig. S9i, j). Therefore, we conclude that NOTCH3 mRNA is a direct substrate of ac4C modification. Additionally, invasion assay showed that NAT10 G641E significantly abolished the effect of NAT10 on cell invasion (Supplementary information, Fig. S9k). Together, our results suggest that NAT10 increases NOTCH3 mRNA stability via ac4C modification.

By analyzing the same tissue microarrays described above, we found that upregulation of NOTCH3 in ESCC was associated with advanced pathological N stage and poor survival in cancer patients (Fig. 7k, l and Supplementary information, Table S13). We further validated that NOTCH3 mRNA ac4C modification was gradually increased from N to T and from T to LN (Fig. 7m). Furthermore, we performed $NaBH_4$ reduction and Sanger sequencing in T, N and LN. The results showed that the C:T mismatches of acPeak region were increased in T and LN compared with N, further confirming that NOTCH3 mRNA is indeed acetylated (Supplementary information, Fig. S9l). In addition, acRIP-qPCR indicated that more NOTCH3 mRNAs were pulled down with the anti-ac4C antibody in SIRT7-knockdown cells, and we obtained the opposite results in KAT7-knockdown cells (Fig. 7n). More importantly, a strong positive correlation between NOTCH3 and NAT10 expression was observed ($P < 0.001$, Fig. 7o), supporting our abovementioned finding that NAT10 positively regulates NOTCH3. We further analyzed datasets from TCGA and found that NOTCH3 mRNA expression was significantly upregulated in esophageal carcinoma cohort (Supplementary information, Fig. S10a). In addition, patients in advanced clinical stages tended to have higher NOTCH3 expression in esophageal cancer (Supplementary information, Fig. S10b). The Boyden chamber invasion assay and animal studies showed that ectopic expression of NOTCH3 significantly abolished the inhibitory effect of NAT10 knockout on cell invasion and metastasis and that knockout of NOTCH3 abrogated the enhancing effect of NAT10 on the invasive potential of ESCC cells and cancer metastasis (Fig. 7p, q). Moreover, NAT10 promoted cell invasion in the presence of WT NOTCH3, but not mutated NOTCH3 (Supplementary information, Fig. S10c). NOTCH3 has been reported to drive the expression of fibronectin.[25] Indeed, we found that NOTCH3 increased the expression of fibronectin mRNA (Supplementary information, Fig. S10d, e). Our results support that NOTCH3 is a substrate of NAT10 and mediates the regulatory effect of NAT10 on cancer metastasis.

Identification of #7586-3507 as a lead compound targeting NAT10 Khib modification to suppress cancer metastasis

To identify the lead compounds that target NAT10 K823-Khib to inhibit cancer metastasis, a virtual screen of a compound library consisting of 1.5 million small molecules was conducted (Fig. 8a). By using the LIBDOCK and CDOCKER algorithms as well as Lipinski's Rule of Five, the top 35 small molecules were selected for further study (Supplementary information, Table S14). Compared with other candidate compounds, #7586-3507 exerted the strongest anti-invasive effects on ESCC cells and showed a significant binding affinity to NAT10 (Fig. 8b–e and Supplementary information, Fig. S11a); thus, we selected this compound as our research focus. The therapeutic efficacy of #7586-3507 in cancer was evaluated in a mouse model. Intragastric administration of #7586-3507 (2.5 mg/kg or 5 mg/kg) led to a significant dose-dependent decrease in metastasis without an obvious change in body weight (Fig. 8f and Supplementary information, Fig. S11b–d). More importantly, #7586-3507 not only inhibited Khib modification and expression of the NAT10 protein (Fig. 8g), but also reduced the ac4C levels in NOTCH3 mRNA in ESCC cells (Fig. 8h). However, #7586-3507 did not affect global Khib level (Supplementary information, Fig. S11e). Mechanistically, #7586-3507 inhibited the interaction between NAT10 and KAT7 (Fig. 8i and Supplementary information, Fig. S11f–h) and subsequently increased NAT10 protein degradation in a ubiquitin-proteasome-dependent manner (Fig. 8j, k and Supplementary information, Fig. S11i). We next investigated whether NAT10 and its K823 site are important for the anticancer bioactivity of #7586-3507. WT NAT10 or the K823R mutant was re-overexpressed in NAT10-deficient KYSE150-Luc-LM5 and EC9706-Luc-LM3 cells (Supplementary information, Fig. S11j). Experiments in cell and mouse models showed that #7586-3507 could not reduce the invasive and metastatic abilities of NAT10-deficient ESCC cells; however, the suppressive effect of #7586-3507 on cancer cell invasion and metastasis was restored when WT NAT10 but not the K823R mutant was overexpressed (Fig. 8l–n and Supplementary information, Fig. S11k). Collectively, these data suggest that #7586-3507 exerts the anticancer bioactivity by inhibiting NAT10 Khib modification.

DISCUSSION

It is increasingly appreciated that PTMs can increase the functional diversity of proteins through regulation of localization, expression and interaction. Since the first discovery of acetylation on histones by Vincent Allfrey in 1964, accumulating groundbreaking discoveries have set the stage for the study of non-histone protein acetylation.[26] However, the biological function and regulatory mechanisms of the newly identified lysine acylation modifications in cancer remain largely unknown. Among the 11 types of new PTMs, Khib attracted our attention due to its marked upregulation in highly metastatic cancer cells. The role of Khib modification in cancer has not been reported. The Khib proteome profiles of 20 paired primary ESCC tumor and metastatic tumor tissues suggested an important role of Khib in cancer metastasis. We quantified 5384 proteins and 39,997 sites with Khib modification, among which 2519 proteins and 6754 sites were differentially modified in metastatic tumors. The Khib proteome data generated here, as a database resource, could provide critical insights into the mechanistic study of cancer and other diseases. Via integration of proteomic analysis with CRISPR/Cas9 functional screening, NAT10 was identified as an important substrate for Khib modification, which mediates its effect on cancer metastasis. Although NAT10 has been reported to play an important role in various cancers, including colorectal cancer[27] and breast cancer,[28] whether NAT10 acts as an acetyltransferase for mRNA ac4C modification to exert its biological function in cancer is unclear, and more importantly, the pattern of lysine acylation in NAT10 protein and its function in cancer are unknown. In the present study, we revealed that Khib modification of NAT10 at K823 may

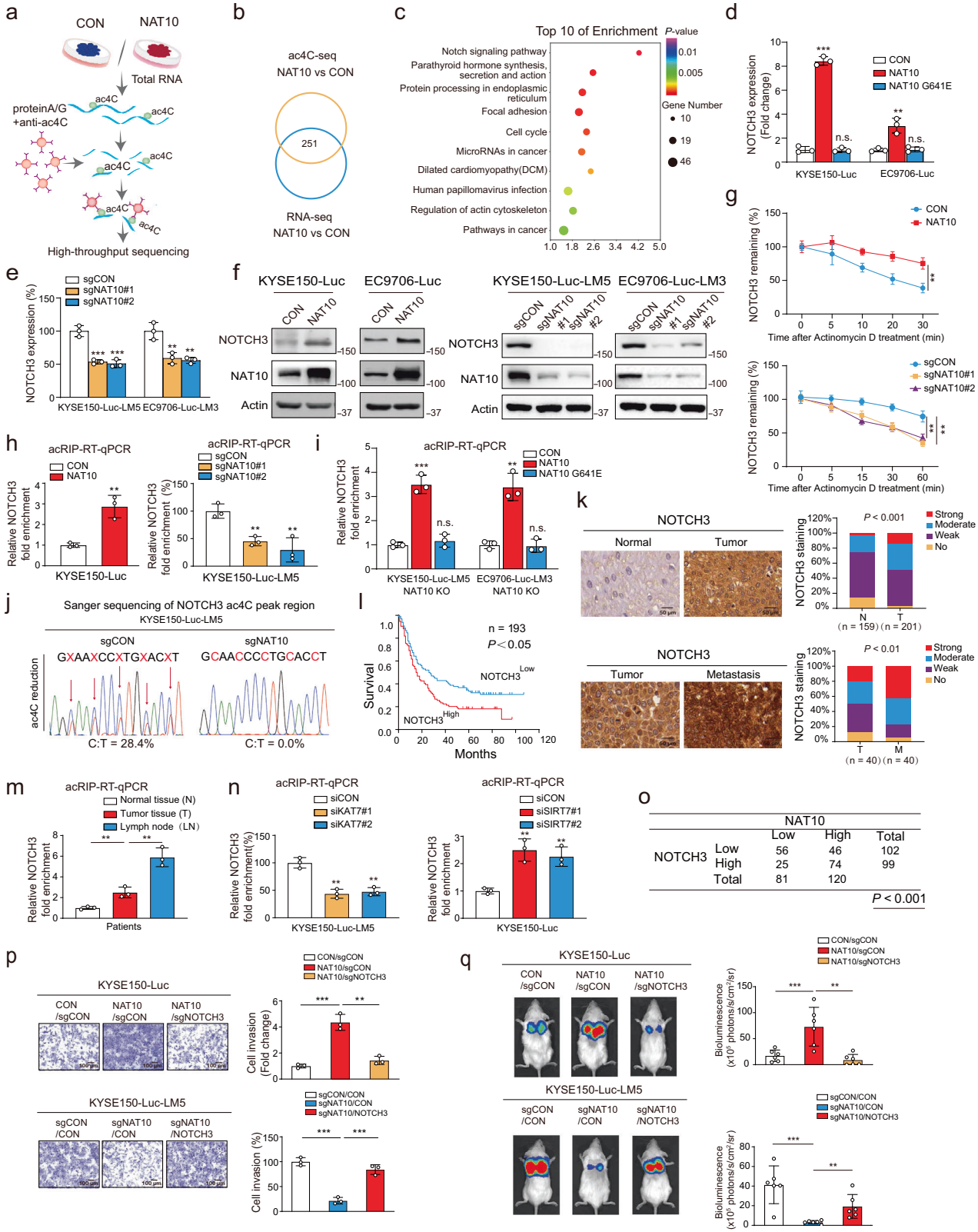

		NAT10		
		Low	High	Total
NOTCH3	Low	56	46	102
	High	25	74	99
	Total	81	120	

$P < 0.001$

play a role in cancer metastasis; specifically, NAT10 823-Khib can be used to predict the prognosis of cancer patients. Identification of the enzymes responsible for protein acylation and deacylation related to Khib modification is important but has not been reported. Here, we uncover for the first time that KAT7 and SIRT7 are the writer and eraser of NAT10 Khib modification, respectively. These findings reveal the molecular mechanism underlying Khib regulation and may open a new avenue for protein function studies and drug development.

The identification of ac4C in mRNA expands the repertoire of epitranscriptomic modifications, with the acetyltransferase NAT10 being the only known enzyme responsible for ac4C deposition in

Fig. 7 NAT10 catalyzes NOTCH3 mRNA ac4C modification to increase its stability. a, **b** Diagram showing the strategy used to investigate the target genes via acRIP-seq and RNA-seq of NAT10-overexpressing cells and control cells. **c** KEGG enrichment analysis showing that genes encoding hyperacetylated mRNAs were enriched mainly in the NOTCH signaling pathway. **d** mRNA level of NOTCH3 when NAT10 WT or NAT10 G641E was overexpressed. **e** mRNA level of NOTCH3 when NAT10 was knocked out. **f** Western blot showing the expression of NOTCH3 when NAT10 expression was modulated. **g** The degradation of NOTCH3 mRNA was monitored when NAT10 expression was modulated. **h** acRIP-qPCR showing the ac4C level in NOTCH3 mRNA when NAT10 was overexpressed or knocked out. **i** acRIP-qPCR showing the ac4C level in NOTCH3 mRNA after transfection with the NAT10 WT or NAT10-G641E mutant. **j** Sanger sequencing showing the NOTCH3 mRNA ac4C peak in WT cells and NAT10-KO cells. **k** Representative images and expression patterns of NOTCH3 in 201 ESCC and 159 paired normal tissues (upper panel) as well as in 40 paired primary tumor and metastatic tumor tissues (lower panel). **l** Kaplan–Meier analysis of overall survival for 193 ESCC patients stratified by tumor NOTCH3 expression. **m** acRIP-RT-qPCR showing the ac4C enrichment in NOTCH3 mRNA in paired N/T/LN samples. **n** acRIP-RT-qPCR showing the ac4C enrichment in NOTCH3 mRNA when KAT7 or SIRT7 was knocked down. **o** Association between NAT10 and NOTCH3 expression in ESCC tissues. **p** Boyden chamber invasion assay showing that knockout of NOTCH3 attenuated the effect of NAT10 on cell invasion. **q** Bioluminescence imaging and quantitative analysis showing that NOTCH3 mediated the effect of NAT10 on ESCC metastasis. Error bars, SDs; n.s. not significant; $^{**}P < 0.01$; $^{***}P < 0.001$.

mammals.[12] Finer mapping and discovery of its substrates and readers are awaited to facilitate functional and mechanistic studies. In the present study, 5187 mRNAs were identified as ac4C substrates by acRIP-seq. Among the 1065 mRNAs exhibiting higher ac4C levels upon NAT10 overexpression, 251 also had upregulated expression (fold change > 2, false discovery rate (FDR) < 0.05), further corroborating a previous report indicating that RNA ac4C modification can affect RNA stability or translation efficiency.[12,29] We revealed that NOTCH3 mRNA is stabilized by NAT10-mediated ac4C modification. Remarkably, NOTCH3 has been shown to function in many aspects of cancer progression.[30] For the first time, we showed that ac4C modification of NOTCH3 mRNA constitutes a key regulatory switch for its function in cancer metastasis.

Targeting PTMs, particularly phosphorylation and ubiquitination, is a strong basis for the exploration of therapeutic strategies and development of potent antitumor drugs.[31] For example, small-molecule inhibitors targeting the proteasome, such as bortezomib, carfilzomib, and ixazomib, have achieved tangible success, and more inhibitors are now approaching clinical trials.[31,32] Despite the lag in related research, targeting protein acetylation by inhibition of its writers, erasers or readers also offers a promising option.[33] Targeting Khib and other new lysine acylation modifications may be a new direction for drug development but has not yet been reported. Here, we revealed that Khib modification of NAT10 increases its binding to the deubiquitinase USP39, which enhances NAT10 protein stability in a ubiquitin-proteasome-dependent manner. In addition, substrates of USP39 were systematically identified for the first time by MS-based ubiquitylome analysis and included 2138 proteins and 4824 ubiquitination sites, providing insights into understanding the action mechanisms of USP39. By integrating molecular docking and a functional screen of a small molecule library, the lead compound #7586-3507 was found to directly target the Khib site in NAT10 and inhibit its binding to USP39 to accelerate NAT10 protein degradation, thereby suppressing mRNA ac4C modification of the downstream effector NOTCH3. These findings open a distinctive therapeutic avenue for cancer treatment and warrant further preclinical study. The findings on the role of KAT7 and SIRT7 in Khib modification broaden the knowledge on the enzymatic activities of the previously annotated HATs and HDACs. Thus, our discovery not only opens a new chapter on the role of lysine acylation in cancer but also provides insights and resources for studying this modification in a broader context of physiological events and human diseases. This study demonstrates the theoretical basis for targeting protein Khib modification and its crosstalk with RNA ac4C modification in drug development.

MATERIALS AND METHODS

Sample preparation

Biospecimens were collected from newly diagnosed patients who underwent surgical resection (Shanghai Chest Hospital, Shanghai Jiao Tong University, Shanghai, China). All sample collection procedures complied with routine clinical practice. Protein sample preparation and liquid chromatography-tandem mass spectrometry (LC-MS/MS) using the Tandem Mass Tag (TMT) were performed at PTM Biolab Co., Ltd. (Hangzhou, Zhejiang, China). Fresh tissue samples were ground into powder under liquid nitrogen, and lysis buffer (8 M urea and 1% protease inhibitor cocktail) was added to lyse cells. This step was followed by three rounds of sonication on ice using a high-intensity ultrasonic processor (for cell sample, it was immediately sonicated three times on ice using a high-intensity ultrasonic processor in lysis buffer). For PTM assays, inhibitors were added to the lysis buffer, e.g., 3 μM trichostatin A (TSA) and 50 mM nicotinamide (NAM) to maintain acetylation. After centrifugation at 12,000× *g* and 4 °C for 10 min, the supernatant was collected, and the protein concentration was determined. For digestion, proteins in the solution were reduced by incubation with 5 mM dithiothreitol for 30 min at 56 °C and alkylated with 11 mM iodoacetamide for 15 min at room temperature in the dark. The protein sample was then diluted with 100 mM triethylammonium bicarbonate (TEAB) to achieve a urea concentration of < 2 M. Finally, trypsin was added at a 1:50 trypsin:protein mass ratio for initial digestion overnight and a 1:100 trypsin:protein mass ratio for a second 4-h digestion.

TMT labeling (for analysis of the cell Khib proteome)

After trypsin digestion, peptides were dissolved in 0.5 M TEAB. Peptides in each channel were labeled with the corresponding TMT reagent (based on the manufacturer's protocol, Thermo Fisher Scientific, Waltham, MA, USA) and incubated for 2 h at room temperature. Five microliters of each sample were pooled, desalted and analyzed by MS to check the labeling efficiency. Then, the labeling reactions were quenched by adding 5% hydroxylamine. The pooled samples were then desalted on a Strata X C18 SPE column (Phenomenex, Torrance, CA, USA) and dried by vacuum centrifugation. Next, the samples were fractionated by high-pH reversed-phase high-performance liquid chromatography (HPLC) using an Agilent 300 Extend C18 column (5 μm particles, 4.6 mm ID, 250 mm length). In brief, peptides were separated on a gradient of 2%–60% acetonitrile in 10 mM ammonium bicarbonate (pH 10) into 80 fractions over 80 min. Then, the peptides were combined into 9 fractions and dried by vacuum centrifugation.

Affinity enrichment

For analysis of the proteome, Khib proteome and ubiquitylome, to enrich modified peptides, tryptic peptides dissolved in NETN buffer (100 mM NaCl, 1 mM EDTA, 50 mM Tris-HCl, pH 8.0, and 0.5% NP-40) were incubated with the appropriate prewashed antibody beads (PTM Biolab Co., Ltd.) at 4 °C overnight with gentle shaking. Then, the beads were washed four times with NETN buffer and twice with water. The bound peptides were eluted from the beads with 0.1% trifluoroacetic acid. Finally, the eluted fractions were combined and vacuum-dried. For LC-MS/MS analysis, the obtained peptides were desalted with C18 ZipTips (Millipore, Bedford, MA, USA) according to the manufacturer's instructions.

LC-MS/MS analysis

For analysis of the cell Khib proteome, the tryptic peptides were dissolved in solvent A (0.1% formic acid, 2% acetonitrile in water) and directly loaded onto ReproSil-Pur Basic C18 (1.9 μm, 100 μm × 25 cm). Peptides were separated with a gradient of 5%–25% solvent B (0.1% formic acid in 90% acetonitrile) over 60 min, 25%–35% in 22 min, climbing to 80% in 4 min then holding at 80% for the last 4 min, all at a constant flow rate of 450 nL/min on an EASY-nLC 1200 UPLC system (Thermo Fisher Scientific). The

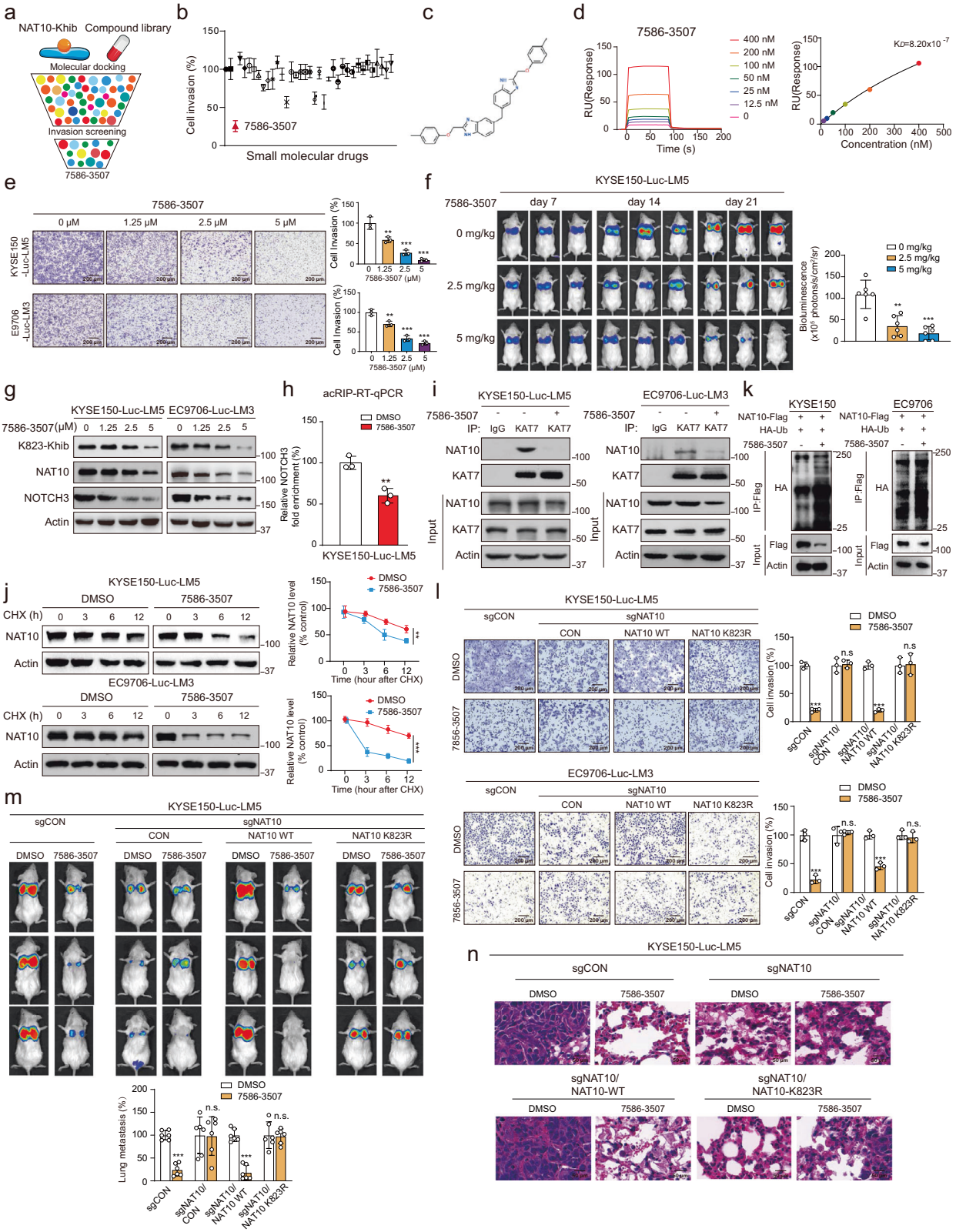

separated peptides were analyzed in Q ExactiveTM HF-X (Thermo Fisher Scientific) with a nano-electrospray ion source. The electrospray voltage applied was 2.0 kV. The full MS scan resolution was set to 120,000 for a scan range of 350–1600 m/z. Up to 20 most abundant precursors were then selected for further MS/MS analyses with 30 s dynamic exclusion. The HCD fragmentation was performed at a normalized collision energy (NCE) of 28%. The fragments were detected in the Orbitrap at a resolution of 15,000. Fixed first mass was set as 100 m/z. Automatic gain control (AGC) target was set at 1E5, with an intensity threshold of 3.3E4 and a maximum injection time of 100 ms.

For analysis of the other proteome stated above, peptides were dissolved in solvent A (0.1% formic acid and 2% acetonitrile in water) and directly

Fig. 8 Pharmacological inhibition of NAT10 by small-molecule compounds offers a therapeutic option. a Diagram showing the approach used to screen NAT10 Khib inhibitors. **b** Quantitative analysis comparing the invasion ability among cells treated with 35 candidate compounds. **c** The chemical structure of #7586-3507. **d** Biacore analysis revealing the binding between the NAT10 protein and #7586-3507. **e** Boyden chamber assay showing the effect of #7586-3507 on cell invasion. **f** Bioluminescence imaging and quantification of lung metastasis showing the dose-dependent suppressive effect of #7586-3507 on metastasis in mice. #7586-3507 was diluted in 2% DMSO, 30% PEG300, 1% Tween 80, and 67% ddH_2O. **g** Effect of #7586-3507 on NAT10 K823-Khib, NAT10 and NOTCH3 protein levels. **h** acRIP-qPCR showing the decreased levels of ac4C in NOTCH3 mRNA in #7586-3507-treated ESCC cells. **i** Co-IP assay showing that #7586-3507 reduced the interaction between NAT10 and KAT7. **j** CHX chase assay showing that the presence of #7586-3507 induced NAT10 protein degradation. **k** The addition of #7586-3507 induced the ubiquitination and degradation of NAT10. **l** NAT10-KO ESCC cells were further transfected with WT NAT10, NAT10 K823R mutant or vector control. For each cell line obtained, invasion ability of #7586-3507-treated cells was compared with that of DMSO-treated cells, respectively. **m** Bioluminescence imaging and quantitative analysis showing that #7586-3507 could not suppress the ability of NAT10-KO cells to form metastatic tumors and that the suppressive effect of #7586-3507 was restored when the cells were reconstituted with WT NAT10 but not NAT10 K823R. For each group obtained, bioluminescence of #7586-3507-treated groups was compared with that of DMSO-treated groups, respectively. **n** H&E staining showing lung metastasis as indicated. Error bars, SDs; n.s. not significant; $^{**}P < 0.01$; $^{***}P < 0.001$.

loaded onto a custom-made reversed-phase analytical column (25 cm length, 75/100 µm i.d.). Peptides were separated with a gradient of 6%–24% solvent B (0.1% formic acid in acetonitrile) over 70 min, 24%–35% over 14 min, increasing to 80% over 3 min and maintained at 80% for the last 3 min. All steps were performed at a constant flow rate of 450 nL/min on a nanoElute ultra-high-performance liquid chromatography (UHPLC) system (Bruker Daltonics, Inc., Billerica, MA, USA). The peptides were subjected to capillary source followed by the timsTOF Pro (Bruker Daltonics) mass spectrometer. The electrospray voltage applied was 1.60 kV. Precursor and fragment ions were analyzed at the time-of-flight (TOF) detector, with an MS/MS scan range of 100–1700 m/z. The timsTOF Pro was operated in parallel accumulation-serial fragmentation (PASEF) mode. Precursor ions with charge states of 0–5 were selected for fragmentation, and 10 PASEF-MS/MS scans were acquired per cycle. The dynamic exclusion setting was 30 s. The resulting MS/MS data were processed using the MaxQuant search engine (v.1.6.15.0). Tandem mass spectra were searched against the human SwissProt database (20,422 entries) concatenated with a reverse decoy database. Trypsin/P was specified as the cleavage enzyme, and up to 2 missed cleavages were allowed. The mass tolerance for precursor ions was set to 20 ppm in the first search and 5 ppm in the main search, and the mass tolerance for fragment ions was set to 0.02 Da. Carbamidomethylation on Cys was specified as the fixed modification, and acetylation on the protein N-terminus and oxidation on Met were specified as the variable modifications. The FDR was adjusted to < 1%.

Generation of the polyclonal rabbit anti-human NAT10 Khib-K823 antibody

The polyclonal rabbit anti-human NAT10 Khib-K823 antibody was developed by PTM Biolab Co., Ltd. and was directed against two synthetic NAT10 peptides with K823-Khib (PYDL-(2ohibutyryl)K-RLEMYSRNC and YDL-(2ohibutyryl)K-RLEMYSRC). Another nonacylated peptide (PYDLKRLEMYSRNC) was also generated and verified by MS analysis. The Khib-modified peptides were then employed to trigger immune responses in pathogen-free barrier facility-raised New Zealand White rabbits (PTM Biolab Co., Ltd.). After immunization, sera were purified using protein A and collected for quality control, including ELISA, dot blot analysis and western blot analysis.

RNA-seq

RNA-seq was performed to compare the gene profiles of NAT10-overexpressing ESCC cells and parental cells (Epibiotek Co., Ltd., Guangzhou, China). We applied the DEGseq package to filter the differentially expressed genes after significance analysis and FDR analysis with the following criteria: 1) fold change > 2; 2) FDR < 0.05.

Tissue microarray and immunohistochemistry

Immunohistochemistry was performed as previously described.[34] Tissue microarrays (Shanghai Outdo Biotech, Shanghai, China) consisting of 201 primary ESCC tumors and 159 matched adjacent normal tissues were used to analyze the levels of NAT10 K823-Khib, NAT10, USP39, NOTCH3, KAT7 and SIRT7. Another tissue microarray containing 40 primary ESCC and matched metastatic tumor tissues (Biomax, Rockville, MD, USA) was applied to detect protein expression in primary and metastatic ESCC tumor tissues. In brief, sections were blocked and incubated with NAT10 (Proteintech, Chicago, IL, USA), K823-Khib (PTM Biolab Co., Ltd.), NOTCH3, KAT7 (Proteintech) or SIRT7 (Affinity Biosciences, Cincinnati, OH, USA) antibodies overnight at 4 °C, and were then incubated with the corresponding biotinylated secondary antibody and peroxidase-conjugated avidin-biotin complex (Dako, Mississauga, ON, Canada). Then, 3,3′-diaminobenzidine (Dako) was used to visualize staining, and the sections were counterstained with H&E. The immunohistochemical staining intensity in the tissue microarray was scored as follows: no staining, 0; weak staining, 1; moderate staining, 2; and strong staining, 3. Samples with a score of 0 or 1 were classified as having low expression, while those with a score of 2 or 3 were classified as having high expression.

Cell culture

The human ESCC cell lines KYSE150 and EC9706 were purchased from DSMZ (Braunschweig, Germany)[35] and maintained in RPMI-1640 medium (Thermo Fisher Scientific) supplemented with 10% fetal bovine serum (FBS) (ExCell Bio, Shanghai, China) in a humidified atmosphere of 5% CO_2 at 37 °C. The highly metastatic cell lines and parental cells were generated as previously described.[36]

Drugs

The small-molecule compounds were obtained from ChemDiv (San Diego, CA, USA). CHX was obtained from Cell Signaling Technology (Beverly, MA, USA). Actinomycin D was purchased from Sigma-Aldrich (St. Louis, MO, USA).

In vitro and in vivo CRISRR/Cas9 selection

To conduct a CRISPR-Cas9 knockout screen, after transduction with the designed sgRNA library, cells were treated with puromycin for 48 h. Then 2×10^7 cells were harvested one week later to obtain input DNA. For in vitro screen, cells were selected by invasion assay. To ensure sgRNA representation, at least 2×10^7 cells were maintained at any given time. The cells that invaded the lower chamber were detached with trypsin and cultured until the amount of the cells was adequate for the next round of invasion selection. Finally, the cells were reseeded into the upper compartment of a new invasion chamber. The same procedure was repeated three times. For in vivo screen, cells were injected intravenously into NCG mice and lung with metastasis were sampled 4 weeks upon injection.

Plasmids, transfection, infection and gene knockout by CRISPR/Cas9 genome editing

Small interfering RNAs (siRNAs) against human KAT7, SIRT7 and USP39 were obtained from Hanyi Biosciences Inc. (Guangzhou, China). siRNAs were transfected into cells using Lipofectamine 3000 (Thermo Fisher Scientific) according to the manufacturer's instructions. The NAT10, USP39, NOTCH3 plasmids and control plasmid were purchased from Hanyi Biosciences Inc. All mutants were generated using a pair of oligonucleotide primers designed with mismatched nucleotides (Supplementary information, Table S15). The annealed sgRNA oligos were inserted into the lentiCRISPRv2 vector (Addgene plasmid 52961),[37] which was a gift from Feng Zhang (Massachusetts Institute of Technology Cambridge, MA, USA), to generate the NAT10 and NOTCH3 knockout plasmids. Transfection, transduction and establishment of stable cell lines were performed as previously described.[38] In brief, plasmid containing the sgRNA targeting NAT10 was co-transfected with the 3rd generation packaging plasmids (Addgene #12251, Addgene #12253, Addgene #12259) into HEK293T cells using Lipofectamine 3000 as previously described. Supernatants were collected 48 h after transfection, centrifuged at 1500 rpm for 5 min, and filtered through a 0.45 µm filter. ESCC cells were infected to express Cas9 and gRNA to produce stable cell lines. After 7 days of puromycin selection (1 µg/mL), the NAT10 protein level was analyzed by western blot assay. The sgRNA and siRNA sequences are listed in Supplementary information, Table S16.

qRT-PCR

Total RNA was extracted using TRIzol reagent (Thermo Fisher Scientific) and reverse transcribed using a PrimeScript II First-Strand cDNA Synthesis Kit (Takara, Dalian, China). Then, qRT-PCR was performed as previously described.[39] Relative gene expression was normalized to GAPDH expression. The primers are listed in Supplementary information, Table S15. To evaluate mRNA stability, cells were treated with 5 μM actinomycin D for 0, 5, 10, 20 and 30 min, and the mRNA half-life was determined.

acRIP-seq and acRIP-qPCR

acRIP-seq was conducted to compare NAT10-overexpressing ESCC cells and parental cells. Total RNA was extracted using TRIzol (Invitrogen). rRNA was removed using a QIAseq FastSelect-rRNA HMR Kit (Qiagen, Hilden, Germany). The fragmented RNA was purified and collected with a Zymo RNA Clean and Concentrator-25 Kit (Zymo Research, Irvine, CA, USA). The anti-ac4C antibody, Dynabeads Protein G (Invitrogen), and purified RNA were incubated at 4 °C for 6 h. The immunoprecipitated RNA was collected according to the manufacturer's instructions. The library was constructed using an EpiTM Mini LongRNA-seq Kit (Epibiotek Co., Ltd., Guangzhou, China) according to the manufacturer's protocol. Quality control of the library was conducted with a Bioptic Qsep100 Analyzer (Bioptic Inc., Taiwan, China). The NovaSeq high-throughput sequencing platform was used for sequencing by Epibiotek Co., Ltd. acRIP-qPCR was performed using an EpiTM ac4C immunoprecipitation kit (Epibiotek Co., Ltd.) following the manufacturer's instructions. In brief, RNA was subjected to magnetic immunoprecipitation with an anti-ac4C antibody. Isolated RNA fragments were subjected to one-step reverse transcription PCR to detect ac4C-modified mRNAs of target genes.

$NaBH_4$ treatment and targeted ac4C sequencing

$NaBH_4$ treatment and targeted ac4C sequencing were performed as described.[9,11,24] In brief, total RNA was extracted using TRIzol reagent (Thermo Fisher Scientific) and treated with 100 mM $NaBH_4$ at 55 °C in the dark for 1 h. Next, $NaBH_4$-treated RNA was purified with miRNeasy Kit (Qiagen, Hilden, Germany) and reverse transcribed using a PrimeScript II First-Strand cDNA Synthesis Kit (Takara). After PCR reaction, the PCR products were purified and subjected to Sanger sequencing (Ruibiotech, Beijing, China). The peak height of each base was measured and the percentage of misincorporation was determined as follows: Percentage of misincorporation = peak intensity of T/sum of C and T base peaks × 100%.

IP-MS and co-IP

Protein digestion and MS analysis were performed as previously described.[40] In brief, NAT10-overexpressing cells were lysed with lysis buffer. Proteins were digested with trypsin, freeze-dried in a vacuum, resuspended in anhydrous acetonitrile solution, and desalted with a MonoTIPTM C18 Pipette Tip (GL Sciences, Tokyo, Japan). Peptide samples were analyzed with an Orbitrap Fusion Lumos mass spectrometer (Thermo Fisher Scientific). Then, raw data were analyzed using Proteome Discoverer (Thermo Fisher Scientific) and Spectronaut (Omicsolution Co., Ltd., Shanghai, China) software. Protein and peptide FDRs were set to 1%. For co-IP, after prewashing with IgG beads (Santa Cruz Biotechnology, Santa Cruz, CA, USA) and protein A/G Sepharose beads (Invitrogen) for 1 h at 4 °C, cell supernatants were incubated first with the appropriate primary antibody overnight at 4 °C and then with protein A/G Sepharose beads for 4 h. Immunoprecipitated proteins were eluted and were then detected by western blotting.

Western blot analysis

Western blot analysis was performed as previously described.[41] The primary antibodies used included pan antibodies against a panel of lysine acylation modifications (PTM Biolab Co., Ltd.), as well as NAT10, USP39, KAT7, SIRT7, NOTCH3, Myc, HA (Proteintech), pan-Khib, K823-Khib (PTM Biolab Co., Ltd.), E-cadherin (BD Biosciences, Bedford, MA, USA), actin (Santa Cruz Biotechnology) and Flag (Sigma-Aldrich) antibodies. The antibodies are listed in Supplementary information, Table S17.

Immunofluorescence

Immunofluorescence staining was performed as described previously.[39] Cells were fixed with 4% paraformaldehyde for 10 min, permeabilized with 0.1% Triton X-100, blocked with 5% BSA, and incubated with a primary antibody followed by the corresponding secondary antibody. Nuclei were counterstained with DAPI, and images were acquired with a laser scanning confocal microscope.

Surface plasmon resonance (SPR) analysis

SPR analysis was performed using a Biacore X100 system (GE Healthcare Life Sciences, Marlborough, MA, USA) as previously described.[42] NAT10 (Origene, Rockville, MD, USA) protein was immobilized onto a CM7 chip (GE Healthcare Life Sciences) by amine coupling. The inhibitors were diluted with running buffer, and the samples were loaded. Biacore analysis software was used for curve fitting, and the K_D values of the inhibitors for the protein were obtained.

Compound screening strategy and molecular docking simulation

For lead compound screening, the 3D model of NAT10 was generated with MODELER protocol in Discovery Studio 4.5 (Accelrys Inc, San Diego, CA, USA). Compounds with poor drug-like properties were first filtered based on the Lipinski Rule of Five and Veber Rule, then the remaining 1,053,106 compounds were subjected to target K823 in NAT10 based on the structure-based virtual screening via the Libdock protocol of Discovery Studio 4.5. The parameters of the active site were set as follows: center_x = 35.4893, center_y = 21.7776, and center_z = 120.2334. 291 ligands were obtained based on the CDOCKER docking programs. After removing isoforms, we selected 35 compounds for further invasion screening. The molecular mechanics Poisson-Boltzmann surface area (MM/PBSA) method was employed to calculate the binding free energies of NAT10 and USP39.

In vitro invasion assays

The invasion assays were conducted with Boyden chambers as previously described.[43] The invasion chamber membrane was coated with Matrigel (BD Biosciences). The cells of interest were resuspended in FBS-free medium and seeded in the upper compartment of the chamber, while complete medium was added to the lower compartment of the chamber as a chemoattractant. The invaded cells were fixed with methanol and stained with 0.2% crystal violet for 5 min.

Luciferase reporter assay

The promoter region of fibronectin was amplified and inserted into the pGL3-Basic plasmid. The luciferase assay was performed using reporter lysis buffer (Promega) and luciferase assay reagent according to the manufacturer's instructions. In brief, cells were co-transfected with the pGL3-fibronectin construct and the NOTCH3 expression plasmid or control plasmid. A renilla luciferase expression vector was used as the internal control. After 48 h, firefly and renilla luciferase activities were measured by using a dual luciferase reporter assay system (Promega) according to the manufacturer's instructions.

Lymph node metastasis mouse model

Mice were inoculated subcutaneously in the hind footpad with 1×10^6 NAT10-overexpressing or NAT10-KO cells. Mice were imaged using an IVIS-100 Imaging System (Caliper Life Sciences, Waltham, MA, USA) after intraperitoneal injection of D-luciferin (150 mg/kg in PBS) under anesthesia for exposure. Tumors removed from sites between the footpad region and the ankle joint were defined as "LN metastases" (local tumor invasion). All footpad tumors were resected and fixed with 10% formaldehyde/PBS for histological analysis. Lymph nodes and footpad tumors were subjected to histological staining.

Experimental metastasis model

This experiment was performed as previously described.[44] In brief, 1×10^6 luciferase-expressing ESCC cells per mouse were injected via the tail vein. Metastasis was monitored weekly using the IVIS-100 Imaging System.

Statistical analysis

All experiments were repeated three times. Statistical analyses were performed by using GraphPad Prism 7.0 (GraphPad Software Inc., La Jolla, CA, USA). Survival analysis was performed by the Kaplan–Meier method with the log-rank test using Statistical Package for the Social Sciences (SPSS) software (SPSS Inc., Chicago, IL, USA). All data are shown as the mean ± SD, and significance was assumed at $P < 0.05$.

REFERENCES

1. Wang, Y., Zhang, J., Li, B. & He, Q. Y. Advances of proteomics in novel PTM discovery: applications in cancer therapy. *Small Methods* **3**, 1900041 (2019).
2. Choudhary, C. et al. The growing landscape of lysine acetylation links metabolism and cell signalling. *Nat. Rev. Mol. Cell Biol.* **15**, 536–550 (2014).

3. Narita, T., Weinert, B. T. & Choudhary, C. Functions and mechanisms of non-histone protein acetylation. *Nat. Rev. Mol. Cell Biol.* **20**, 156–174 (2019).
4. Deng, G. et al. Loss of heterozygosity and p53 gene mutations in breast cancer. *Cancer Res.* **54**, 499–505 (1994).
5. Johnson, L. et al. Somatic activation of the K-ras oncogene causes early onset lung cancer in mice. *Nature* **410**, 1111–1116 (2001).
6. Birkbak, N. J. et al. Telomeric allelic imbalance indicates defective DNA repair and sensitivity to DNA-damaging agents. *Cancer Discov.* **2**, 366–375 (2012).
7. Zhang, X. et al. Dissecting esophageal squamous-cell carcinoma ecosystem by single-cell transcriptomic analysis. *Nat. Commun.* **12**, 5291 (2021).
8. Yang, Y. M. et al. Advances in targeted therapy for esophageal cancer. *Signal Transduct. Target. Ther.* **5**, 229 (2020).
9. Bortolin-Cavaillé, M. L. et al. Probing small ribosomal subunit RNA helix 45 acetylation across eukaryotic evolution. *Nucleic Acids Res.* **50**, 6284–6299 (2022).
10. Sharma, S. et al. Yeast Kre33 and human NAT10 are conserved 18S rRNA cytosine acetyltransferases that modify tRNAs assisted by the adaptor Tan1/THUMPD1. *Nucleic Acids Res.* **43**, 2242–2258 (2015).
11. Sas-Chen, A. et al. Dynamic RNA acetylation revealed by quantitative cross-evolutionary mapping. *Nature* **583**, 638–643 (2020).
12. Arango, D. et al. Acetylation of cytidine in mRNA promotes translation efficiency. *Cell* **175**, 1872–1886.e24 (2018).
13. Zhang, H. et al. Ketogenesis-generated beta-hydroxybutyrate is an epigenetic regulator of CD8(+) T-cell memory development. *Nat. Cell Biol.* **22**, 18–25 (2020).
14. Simithy, J. et al. Characterization of histone acylations links chromatin modifications with metabolism. *Nat. Commun.* **8**, 1141 (2017).
15. Fang, Y. et al. Histone crotonylation promotes mesoendodermal commitment of human embryonic stem cells. *Cell Stem Cell* **28**, 748–763.e7 (2021).
16. Huang, H. et al. Landscape of the regulatory elements for lysine 2-hydroxyisobutyrylation pathway. *Cell Res.* **28**, 111–125 (2018).
17. Dominissini, D. & Rechavi, G. N(4)-acetylation of cytidine in mRNA by NAT10 regulates stability and translation. *Cell* **175**, 1725–1727 (2018).
18. Xu, W. S., Parmigiani, R. B. & Marks, P. A. Histone deacetylase inhibitors: molecular mechanisms of action. *Oncogene* **26**, 5541–5552 (2007).
19. Tang, X. et al. SIRT7 antagonizes TGF-β signaling and inhibits breast cancer metastasis. *Nat. Commun.* **8**, 318–318 (2017).
20. MacPherson, L. et al. HBO1 is required for the maintenance of leukaemia stem cells. *Nature* **577**, 266–270 (2020).
21. Li, X. et al. Deubiquitinase USP39 and E3 ligase TRIM26 balance the level of ZEB1 ubiquitination and thereby determine the progression of hepatocellular carcinoma. *Cell Death Differ.* **28**, 2315–2332 (2021).
22. Wu, J. et al. USP39 regulates DNA damage response and chemo-radiation resistance by deubiquitinating and stabilizing CHK2. *Cancer Lett.* **449**, 114–124 (2019).
23. Liu, X. et al. NAT10 regulates p53 activation through acetylating p53 at K120 and ubiquitinating Mdm2. *EMBO Rep.* **17**, 349–366 (2016).
24. Arango, D. et al. Direct epitranscriptomic regulation of mammalian translation initiation through N4-acetylcytidine. *Mol. Cell* **82**, 2797–2814.e11 (2022).
25. van Nes, J. et al. A NOTCH3 transcriptional module induces cell motility in neuroblastoma. *Clin. Cancer Res.* **19**, 3485–3494 (2013).
26. Allfrey, V. G., Faulkner, R. & Mirsky, A. E. Acetylation and methylation of histones and their possible role in the regulation of RNA synthesis. *Proc. Natl. Acad. Sci. USA* **51**, 786–794 (1964).
27. Zhang, H. et al. GSK-3beta-regulated N-acetyltransferase 10 is involved in colorectal cancer invasion. *Clin. Cancer Res.* **20**, 4717–4729 (2014).
28. Liu, H. Y. et al. Acetylation of MORC2 by NAT10 regulates cell-cycle checkpoint control and resistance to DNA-damaging chemotherapy and radiotherapy in breast cancer. *Nucleic Acids Res.* **48**, 3638–3656 (2020).
29. Tsai, K. et al. Acetylation of cytidine residues boosts HIV-1 gene expression by increasing viral RNA stability. *Cell Host Microbe* **28**, 306–312.e6 (2020).
30. Majumder, S. et al. Targeting Notch in oncology: the path forward. *Nat. Rev. Drug Discov.* **20**, 125–144 (2021).
31. Deng, L. et al. The role of ubiquitination in tumorigenesis and targeted drug discovery. *Signal Transduct. Target. Ther.* **5**, 11 (2020).
32. Harrigan, J. A., Jacq, X., Martin, N. M. & Jackson, S. P. Deubiquitylating enzymes and drug discovery: emerging opportunities. *Nat. Rev. Drug Discov.* **17**, 57–78 (2018).
33. Fioravanti, R. et al. Targeting histone acetylation/deacetylation in parasites: an update (2017–2020). *Curr. Opin. Chem. Biol.* **57**, 65–74 (2020).
34. Xu, W. W. et al. Cancer cell-secreted IGF2 instigates fibroblasts and bone marrow-derived vascular progenitor cells to promote cancer progression. *Nat. Commun.* **8**, 14399 (2017).
35. Shimada, Y. et al. Characterization of 21 newly established esophageal cancer cell lines. *Cancer* **69**, 277–284 (1992).
36. Liao, L. et al. Anti-HIV drug elvitegravir suppresses cancer metastasis via increased proteasomal degradation of m6A methyltransferase METTL3. *Cancer Res.* **82**, 2444–2457 (2022).
37. Sanjana, N. E., Shalem, O. & Zhang, F. Improved vectors and genome-wide libraries for CRISPR screening. *Nat. Methods* **11**, 783–784 (2014).
38. Tan, X. P. et al. Lomerizine 2HCl inhibits cell proliferation and induces protective autophagy in colorectal cancer via the PI3K/Akt/mTOR signaling pathway. *MedComm* **2**, 453–466 (2021).
39. Zheng, C. C. et al. Targeting PFKL with penfluridol inhibits glycolysis and suppresses esophageal cancer tumorigenesis in an AMPK/FOXO3a/BIM-dependent manner. *Acta Pharm. Sin. B* **12**, 1271–1287 (2022).
40. Hu, H. F. et al. Anti-allergic drug azelastine suppresses colon tumorigenesis by directly targeting ARF1 to inhibit IQGAP1-ERK-Drp1-mediated mitochondrial fission. *Theranostics* **11**, 1828–1844 (2021).
41. Xu, W. W. et al. IGF2 induces CD133 expression in esophageal cancer cells to promote cancer stemness. *Cancer Lett.* **425**, 88–100 (2018).
42. Xu, W. W. et al. Direct targeting of CREB1 with imperatorin inhibits TGFβ2-ERK signaling to suppress esophageal cancer metastasis. *Adv. Sci.* **7**, 2000925 (2020).
43. Xu, W. W. et al. Genome-wide identification of key regulatory lncRNAs in esophageal cancer metastasis. *Signal Transduct. Target. Ther.* **6**, 88 (2021).
44. Hu, H. F. et al. Identification of miR-515-3p and its targets, vimentin and MMP3, as a key regulatory mechanism in esophageal cancer metastasis: functional and clinical significance. *Signal Transduct. Target. Ther.* **5**, 271 (2020).

ACKNOWLEDGEMENTS

This work was supported by the National Key R&D Program of China (2021YFC2501000, 2021YFC2501900), the National Natural Science Foundation of China (82273141, 82073196, 31961160727, 81973339, 82071372), Key Laboratory of Guangdong Higher Education Institutes (2021KSYS009), the Outstanding Scholar Program of Bioland Laboratory (2018GZR110102002), and the Science and Technology Program of Guangzhou (202007030012). We thank Profs. Didier Trono and Vladislav Verkhusha for the plasmids obtained from Addgene.

AUTHOR CONTRIBUTIONS

B.L. conceived and designed the study; L.L., Y.H., S.J.L., X.M.Y., Z.C.L., Y.Y.L., J.Y., G.G.Z., C.M.D., X.W., Y.D.Z., T.Y.X. and C.C.Z. acquired, analyzed and interpreted the data; L.L., Y.H., S.J.L. and X.M.Y. performed statistical analysis and drafted the manuscript; H.Y., C.C., A.L., Z.G.L. and J.B.L. provided technical and/or material support and critically revised the manuscript for important intellectual content; B.L. supervised the study. All authors edited and approved the final version of the manuscript.

COMPETING INTERESTS

The authors declare no competing interests.

ETHICAL APPROVAL

All animal experiments were approved by the Ethics Committee for Animal Experiments of Guangzhou Medical University (G2022-084), and mice were cared under standard conditions according to institutional guidelines. The human ESCC specimens were collected in accordance with the Declaration of Helsinki and was approved by the Ethics Committee of Shanghai Chest Hospital, Shanghai Jiao Tong University (No. KS(Y)22278). Informed consent was obtained from each participant.

ADDITIONAL INFORMATION

Supplementary information The online version contains supplementary material available at https://doi.org/10.1038/s41422-023-00793-4.

Correspondence and requests for materials should be addressed to Bin Li.

Reprints and permission information is available at http://www.nature.com/reprints

Springer Nature or its licensor (e.g. a society or other partner) holds exclusive rights to this article under a publishing agreement with the author(s) or other rightsholder(s); author self-archiving of the accepted manuscript version of this article is solely governed by the terms of such publishing agreement and applicable law.